Benito, M. B., Arroyo Solórzano, M., Climent, A., Montero, W., Alvarado, G. E., López, A., García-Lanchares, C., Marchamalo, M., Ornelas, A., Hernández-Rubio, O., Quirós, L. (2025): Seismic hazard scenarios for the city of San José, Costa Rica: Evaluation of critical ruptures on nearby faults. - Earthquake Spectra, 41, 3, 2335-2370.

https://doi.org/10.1177/87552930251319736

Seismic Hazard Scenarios for the City of San José, Costa Rica: Evaluation of Critical Ruptures on Nearby Faults

María Belén Benito[1*], Mario Arroyo-Solorzano[1,2], Alvaro Climent [3], Walter Montero[4] Guillermo E. Alvarado[4], Allan López[5], Carlos García-Lanchares[6,7], Miguel Marchamalo[6,7], Adriana Ornelas[1], Orlando Hernández-Rubio[1] and Ligia Quirós[1].

[1] Escuela Técnica Superior de Ingenieros en Topografía, Geodesia y Cartografía (ETSITGC), Universidad Politécnica de Madrid (UPM), Spain.

[2] Helmholtz Centre Potsdam, GFZ German Research Centre for Geosciences and University of Potsdam, Germany.

[3] Red Sismológica Nacional de Costa Rica (RSN), San José, Costa Rica.

[4] Centro de Investigaciones en Ciencias Geológicas, Universidad de Costa Rica, San Pedro, Costa Rica.

[5] Escuela de Ingeniería Civil, Universidad Latina de Costa Rica.

[6] Topography and Geomatics Lab. Escuela Técnica Superior de Ingenieros en Caminos, Canales y Puertos, Universidad Politécnica de Madrid, Spain.

[7] Detektia Earth Surface Monitoring S.L. Madrid. Spain.

(*) Corresponding author: María Belén Benito, mariabelen.benito@.upm.es, ETSITGC, UPM, Calle Mercator, 2, 28031 Madrid, Spain

Abstract

Costa Rica has several active shallow (depth < 15 km and Mw > 5.3) crustal faults near towns with high seismic hazard. We present three critical deterministic hazard scenarios in San José city for the Bello Horizonte, Cipreses, and Río Azul faults systems, with Mw 6.2, 6.3 and 6.6, and closest distances to the rupture surfaces of 5.0 km, 4.3 km and 5.2 km, respectively (from the capital center). We estimate accelerations in rock and soil conditions using adapted amplification factors. The results show Peak Ground Acceleration values reaching 0.6 - 0.8g in San José and the Gran Área Metropolitana of Costa Rica, including soil conditions, the scenarios for the Cipreses and Río Azul faults being the most hazardous. We also estimated the response spectra for specific locations, comparing them with those spectra based on the seismic code for Costa Rica. We found that the code spectra were exceeded for rigid and medium soils in short structural periods, but they were conservative for softer soils. Finally, to highlight the relevance of our scenarios, we estimated the deformation using InSAR techniques and a potential fault reactivation assessment by analyzing slip and dilation stress tendencies. The small deformation observed (< 3mm/year) compared with nearby deformation in the Aguacaliente-Navarro fault systems (over 1 cm/year), could indicate either gradual stress accumulation or that scarce energy is being released seismically. Furthermore, analyses of the stress tendencies in the 3 faults indicate a high potential fault reactivation in a short-medium term hazard. San José has not suffered severe earthquake destruction in the last 500 years, although the occurrence of an earthquake such as the scenarios modeled could cause significant losses given the high exposure and vulnerability of the city. Our results provide a further step in seismic risk assessment for San José aimed at development of mitigation measures.

Key Words: Faults, Maximum magnitude, Site effects, Seismic hazard, Stress state, Seismic code, San José Metropolitan Area, DSHA, Seismic scenario, Central America.

1 INTRODUCTION

Costa Rica is characterized by high seismicity of intermediate magnitude earthquakes ($5.0 \leq Mw \leq 7.7$). This earthquake activity is mainly generated in the subduction zone between the Cocos and Caribbean plates, and along the volcanic arc faults. The Gran Área Metropolitana (GAM), which is the most populated region in Costa Rica, including San José (the country's capital), has been affected by numerous destructive earthquakes throughout its history, due to its location surrounded by the complex fault system of the Central Valley. The GAM has approximately 2.6 million inhabitants (approximately 60% of the country's population) and an area of 2044 km^2 (slightly over 4% of Costa Rica's total area).

Several earthquakes of epicentral intensity greater than VIII have occurred on faults in the Central Valley and have caused destruction in towns in the GAM, such as Cartago and Heredia, although there are no reports of major damage in the Central Cantón of San José (CCSJ), the political and socio -economical heart of Costa Rica since 1823. However, some active fault systems near the CCSJ, located within the GAM, could generate critical hazard scenarios in the CCSJ. Furthermore, given the conditions of exposure and vulnerability, which currently exist in this population center, these scenarios could also be critical in terms of seismic risk, leading to significant human and material losses.

In this research, we analyze and characterize critical scenarios that could be generated on faults close to the city of San José. We identify the local faults and their possible maximum magnitudes, highlighting three critical scenarios with high hazard for the city. We then simulate the corresponding expected ground motions using a deterministic approach. Accelerations were simulated firstly at generic rock sites, applying different Ground Motion Prediction Equations (GMPEs) considered suitable for the region. Data compiled from different sources were then used to create a soil conditions map, considering the classification proposed by the National Earthquake Hazards Reduction Program (NEHRP, 2020), so that the ground motions were characterized for the three proposed scenarios, including the local effect. Finally, we characterize the three critical scenarios in terms of PGA and response spectra, considering the soil conditions.

Our results are of particular interest with regard to assessing and calibrating the building design code in the country's capital and subsequently determining the seismic risk, thus facilitating the development of suitable emergency plans and mitigation measures. Bearing in mind the abovementioned situation, this research seeks to quantify the accelerations that can be expected in the CCSJ due to critical ruptures on nearby faults, in turn providing a basis on which to subsequently quantify the associated losses and adopt the necessary mitigation measures.

In addition to simulating the expected motions, a complementary approach was carried out aimed at evaluating the deformation rates in the CCSJ (using MT-INSAR techniques) and the slip-dilatation stress tendencies of the three faults analyzed in the study area, with the objective of compiling data that provides an idea of the slip rate accumulating and the potential for reactivation of these faults.

2 TECTONIC FRAMEWORK AND RISK FACTORS

2.1 SEISMOTECTONIC CHARACTERISTICS

The tectonic framework of Costa Rica is characterized by its location on the southwestern part of the Caribbean Plate, where the Pacific coast is deformed by the subduction of the Cocos Plate under the Caribbean Plate and Panama Microplate (Fig. 1) (Protti et al., 1995; DeMets et al., 2010) and where a significant deformation in the forearc has developed over time (Fisher et al., 2004; Sak et al., 2009; Morell et al., 2012; Mescua et al., 2017). DeMets et al. (2010) identified differences in the convergence rates, with a range of 85-87 mm/year in the north and up to 92- 95 mm/year in the south of Costa Rica.

On the southeastern side of the Caribbean plate is the Panama Microplate. A zone of crustal deformation exists at the boundary of the Panama Microplate with the Caribbean plate to the north, where many authors have pointed to an incipient subduction of the Caribbean plate under the Panama microplate (e.g., Alvarado et al., 2017; Arroyo and Linkimer, 2021b; Bourke et al., 2023). To the south of the Panama microplate, there is also a ‘triple point’ where the Cocos and Nazca plates are separated by the Panama Fracture Zone (PFZ), a transform fault that is subducted under the Panama

Microplate. Furthermore, on the western side of the Caribbean plate is the Central American Sliver (CAS) (i.e., Montero et al., 2017; Araya and Biggs, 2020), which moves at a rate of about 9 to 14 mm/year towards the northwest and parallel to the Middle America Trench. The origin of the CAS is related to the oblique convergence between the Cocos and Caribbean plates or to the collision of the Cocos Ridge with southern Costa Rica (LaFemina et al., 2009; Fig. 1).

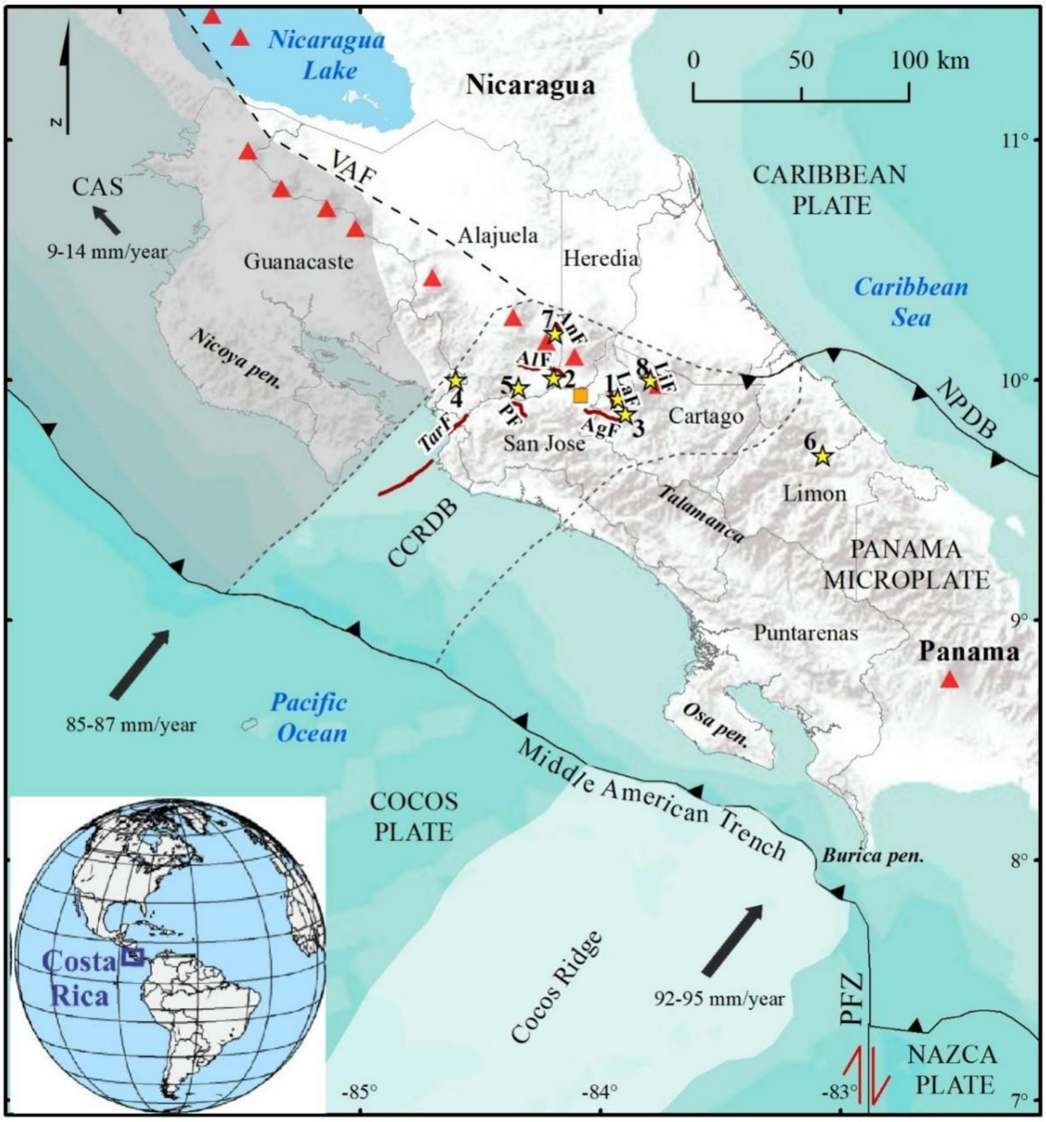

Figure 1. Tectonic framework of Costa Rica. The grey-shaded area corresponds to the Central America Sliver (CAS), and the region within the dotted lines represents the Central Costa Rica Deformed Belt (CCRDB). The thicker dotted line, located next to the VAF label, represents the simplified northeastern boundary of the Central American Forearc Block along the Volcanic Arc Faults. NPDB is the North Panama Deformed Belt, and PFZ is the Panama Fracture Zone. The red triangles represent the Quaternary volcanoes along the volcanic arc, the orange square represents downtown San José, and the numbered stars represent the most relevant earthquakes for central Costa Rica mentioned in the text: 1) 1841 Mw 6.4 San Antolín, 2) 1888 Mw 6.0 Fraijanes, 3) 1910 Mw 6.4 Cartago, 4) 1924 Mw 7.0 Orotina, 5) 1990 Mw 5.7 Piedras Negras, 6) 1991 Mw 7.7 Limón, 7) 2009 Mw 6.2 Cinchona, and 8) 2016 Mw 5.5 Capellades. The faults mentioned in the text and associated

with these earthquakes are shown in red and labeled as AgF: Aguacaliente Fault, AlF: Alajuela Fault, AnF: Ángel Fault, LaF: Lara Fault, LiF: Liebres Fault, PF: Picagres Fault, and TarF: Tárcoles Fault.

Central Costa Rica could be subdivided into an internal forearc, with a predominance of Neogene sedimentary and volcanoclastic rocks (Denyer and Arias, 1991), and an external forearc, characterized by the presence of Paleogene and Neogene volcanic and sedimentary rocks (Denyer and Alvarado, 2007). The Central Valley of Costa Rica and specifically, the city of San José, is framed within a diffuse plate boundary zone called the Central Costa Rica Deformed Belt (CCRDB) (Fig. 1), where the Caribbean plate, the CAS, and the Panama microplate interact (Montero et al., 2013; Montero et al., 2017). Much of the seismicity in central Costa Rica is shallow and closely related to a complex fault system within the CCRDB, considered the western boundary of the Panama Microplate (Fan et al., 1991; Marshall et al., 2000). This is a transpressive deformation zone that includes sinistral strike-slip faults with strikes E-W to ENE, dextral faults with NW to N strikes, and thrust faults with WNW strikes (Marshall et al., 2000; Montero, 2001).

2.2 RISK FACTORS IN THE CENTRAL CANTÓN OF SAN JOSÉ (CCSJ)

Masonry and precast reinforced concrete are the most common building typologies in Costa Rica (Calderon and Silva, 2019). Approximately 1.18 million structures have been identified and classified into 34 building classes, with more than 97% contained within 15 classes of low-rise structures of reinforced masonry, wood, and precast reinforced concrete. Previous probabilistic seismic vulnerability and risk assessments identified the most significant loss potential for Costa Rica as being mainly concentrated in the Central Valley in the GAM, which embraces four of the seven provincial capitals (Calderon and Silva, 2019). The estimated average annual losses in this region exceed 1 million USD in more than 20 districts. The CCSJ is part of the San José province with an area of 45 km^2, representing approximately 0.1% of the country's total territory. It is the most important city in terms of commercial activity and population, with an estimated population of around ~349,000 inhabitants (INEC, 2021), a housing stock made up of ~73,000 residences (Calderon and Silva, 2019) and a population density of 7,700 inhabitants/km^2. This canton is highly urbanized, with only 3% of its urban land available for construction.

According to the National Census of 2011, 63.4% of the buildings in the CCSJ were in good condition, 29.1% fair, and 7.5% were in poor condition. If the data from the 2011 census is compared to that of the 1973 census, a generalized decrease in the relative proportion of dwellings in good condition can be observed in almost all districts of CCSJ, along with a decrease in the number of dwellings in poor condition, and an increase in those in fair condition (INEC, 2011).

As regards the vulnerability of the CCSJ, it should also be mentioned that much of the building stock was built prior to the seismic resistance regulations which came into force in 1974 (Alvarado and Cordero, 2021) and that almost 25% of the buildings are self-built and therefore lack seismic resistant design (CFIA, 2022). In summary, given the high seismic potential of the Central Valley faults along with the high degree of vulnerability and exposure of the CCSJ, the high seismic risk to which the country's capital is exposed can be affirmed.

3 SEISMIC BACKGROUND

3.1. SOME SIGNIFICANT HISTORICAL EARTHQUAKES NEAR SAN JOSÉ

One of the most damaging earthquakes affecting the CCSJ occurred on September 2, 1841, with an estimated magnitude of Mw 6.4 (Figs. 1, 2 and 3). Known as the San Antolín earthquake it destroyed the city of Cartago, at epicental distance (Rep) around 6 km with a maximum intensity of IX in Modified Mercalli intensity scale (I_{MM}). In San José, the intensity I_{MM} was between VII and VIII with 36 fatalities being recorded. Based on this earthquake, the first construction regulations were developed in the country (Alvarado and Cordero, 2021). The San Antolín earthquake was associated with the Lara fault (Fig. 3), east of San José (Peraldo and Montero, 1999). Another important earthquake occurred in the Central Valley on December 30, 1888, with I_{MM} VIII and Mw 6.0 (Figs. 1,2 and 3). Maximum intensity was observed at Rep 4 km. This earthquake is known as the Fraijanes earthquake and it caused severe destruction in the northern part of the Alajuela fault (Fig. 3), (Alvarado et al, 1988). More recently, Montero et al. (2010) associated the 1888 Fraijanes earthquake with the central sector of the Ángel fault (Fig. 1).

On May 5, 1910, one of the most memorable earthquakes of the 20th century occurred, with epicentral intensity I_{MM} VIII and Mw 6.4. The earthquake destroyed the city of Cartago, located at 6 km from the epicenter, causing ~600 victims (including both the dead and missing), along with 5000 injured (Figs. 1 and 2). This event was felt practically throughout all of Costa Rica. The intensities for the CCSJ, as well as for several areas of Heredia and Alajuela, were reported up to I_{MM} V (Montero and Imamura, 1981). This earthquake is thought to have originated from the Aguacaliente fault (Fig. 3), which is located south of Cartago (Montero and Miyamura, 1981; Montero et al., 2005). Another important earthquake that affected the central Pacific side of the country and the Central Valley was the Orotina event, which occurred on March 4, 1924, and had a maximum I_{MM} of X (Rep 10 km) and Mw 7.0 (Figs. 1 and 2). This earthquake occurred beyond the Central Valley but affected the CCSJ, causing extensive damage to the civil infrastructure and it was associated with the Tárcoles fault (Montero, 1999), although some other authors consider that it was most likely to have been a subduction event (Arroyo-Solorzano and Linkimer, 2021).

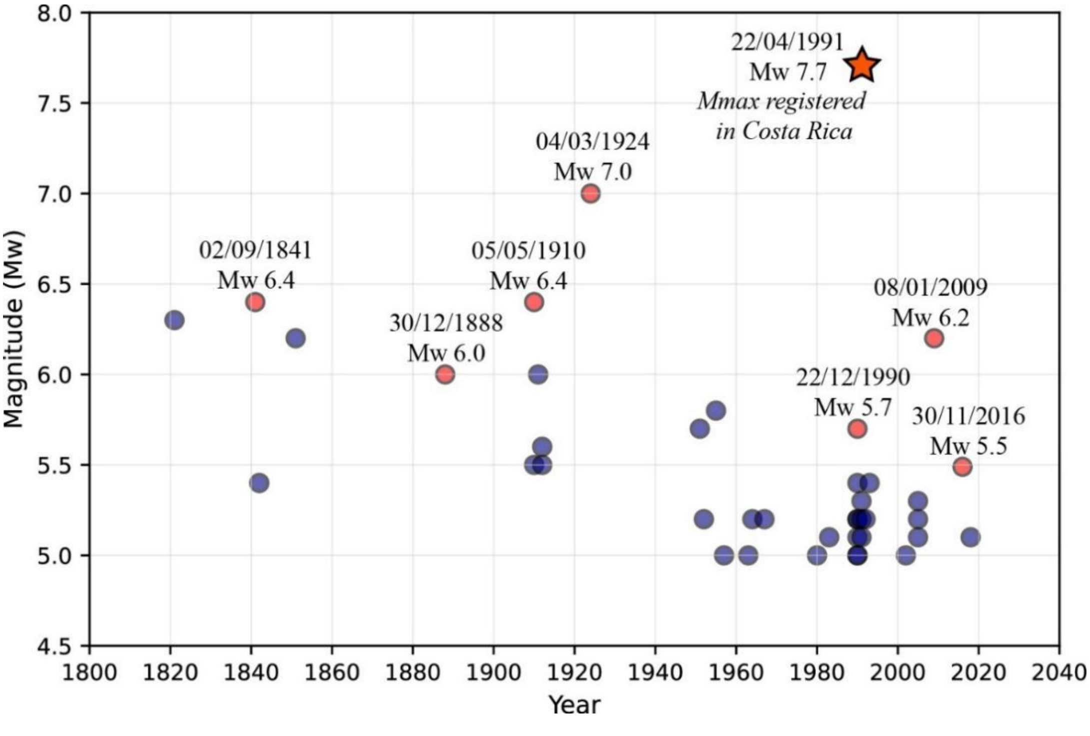

Figure 2. Temporal evolution of the seismicity originated from crustal faults in the Costa Rica seismic zone C6 (Central Valley and Volcanic Range; Alvarado et al., 2017) with magnitudes Mw ≥ 5. The red circles correspond to the events highlighted in the text, and the star corresponds to the earthquake with the highest magnitude registered in Costa Rica.

Hence, over the last 200 years, four destructive earthquakes (1841, 1888, 1910, and 1924) have taken place either within or near the Central Valley (Fig. 3). These earthquakes, all of Mw > 6.0 (Figs. 1, 2 and 3), seriously affected the CCSJ although they did not cause severe destruction in the capital city. Those earthquakes occurred over a period of less than 100 years. However, in the last century there have been no earthquakes greater than Mw 6.0 in the Central Valley, where only two relevant events, one of Mw 5.7 and the other 5.5, have occurred (Fig. 3).

On December 22, 1990, the Mw 5.7 Piedras Negras earthquake occurred in the southern part of Alajuela (Figs. 1, 2 and 3), resulting in intensities from VI to VII in the western part of CCSJ (Rep 12 km). This earthquake was attributed to the Picagres fault (Montero and Rojas, 2014). Another event occurred on April 22, 1991, known as the Limón earthquake (Mw 7.7), this being the maximum instrumentally measured earthquake magnitude in Costa Rica (Figs. 1 and 2) (Arroyo-Solorzano and Linkimer 2021; RSN, 2021), with a maximum intensity of I_{MM} X at 25 km from the epicenter . This earthquake was highly destructive and caused severe losses on the Caribbean side, including 102 deaths and 582 people injured. It originated in a major seismic source at the North Panama Deformed Belt (NPDB) (Fig. 1), where incipient subduction of the Caribbean plate under the Panama microplate is postulated (e.g., Alvarado et al., 2017; Arroyo and Linkimer, 2021; Bourke et al., 2023).

Finally, the most recent relevant events in Central Costa Rica were the January 8, 2009 (Mw 6.2) Cinchona earthquake and the November 30, 2016 (Mw 5.5) Capellades earthquake (Figs. 1, 2 and 3). The former occurred on the northern slopes of the Poás volcano, associated with a northern branch of the Ángel fault (Montero et al., 2010), and had a maximum intensity I_{MM} IX at epicentral distance of 6 km, causing 25 deaths, 15 missing and 300 people injured. It caused great destruction to the infrastructure and roads around the epicentral zone (Barquero et al., 2009). The Capellades earthquake occurred in the proximity of the Turrialba and Irazú volcanoes and allowed a previously unmapped fault to be defined; namely the Liebres fault (Linkimer et al., 2018). The maximum intensity report estimated I_{MM} to be VI in the epicentral area, where damage to several houses, landslides and falling objects were reported (RSN, 2021).

3.2. PREVIOUS SEISMIC HAZARD STUDIES IN COSTA RICA (ESTIMATES IN ROCK CONDITIONS)

Several previous studies concerning seismic hazard assessment, both deterministic and probabilistic, are worthy of mention. The first hazard study in Central America was carried at national scale by the John Blume Earthquake Engineering Center, of Stanford University, California, in the mid-1970s. In Costa Rica, Mortgat et al. (1977), carried out the first study using a probabilistic methodology, which resulted in isoacceleration (PGA) and isoduration maps for return periods (RP) of 50, 100, 500 and 1000 years. These maps provided the basis for the Seismic Code of Costa Rica of 1986 (CFIA, 1987). The PGA value for San José was 0.31 g for a RP of 500 years.

Laporte et al. (1994) subsequently carried out a probabilistic study (using a logic tree) at national level, employing an attenuation model developed for the Central American region (Climent et al., 1994). Their results included PGA maps for RP of 50, 100, 500, and 1000 years, hazard curves for San José and Golfito, as well as uniform hazard pseudo-velocity spectra. In the case of San José, a PGA value of 0.37 g was estimated for a RP of 500 years.

Rojas et al. (1998) implemented a probabilistic assessment combining fifteen seismic source areas and five active fault systems, using the attenuation model of Schmidt et al. (1997). This study produced three PGA maps for the Central Valley, for return periods of 50, 100 and 500 years, obtaining a PGA value for San José of 0.53 g for a RP of 500 years. Fernández and Rojas (2000) published a Costa Rica seismic hazard map for a 500-year RP, based on 21 crustal and 2 intraplate seismic source areas. They applied the attenuation models of Schmidt et al. (1997) and obtained a PGA of 0.42 g for the city of San José. Another national study was carried out by Rojas et al. (2005) for the National Insurance Institute (INS), which included 36 seismic zones, divided into 27 crustal sources and 9 related to the subduction (interplate and intraplate). A PGA value of 0.51 g was estimated for San José for a RP of 500 years. Studies prior to 2002 were considered for the 2003 updating of the Seismic Code of Costa Rica (CFIA, 2003) using a minimum RP of 500 years for the design.

Another hazard study was carried out within the framework of the RESIS II Project (Benito et al., 2010; Benito et al., 2012). This was also a zoned probabilistic study for Central America, considering crustal, interplate and intraplate subduction zones on a national scale, resulting in PGA maps for RP of 500, 1000, and 2500 years. In the case of the metropolitan area of San José, the PGA values estimated in that study were around 500 gal for a RP of 500 years, similar to the value estimated by Rojas et al. (1998) and Rojas et al. (2005), although slightly higher than the estimations by Laporte et al. (1994) and Fernández and Rojas (2000). A dominant earthquake in San José for a RP of 500 years, characterized by the magnitude-distance pair (Mw = 6.5, R = 0 - 15 km) was also determined through disaggregation analysis as part of the RESIS II project. According to this analysis, some local faults in the Central Valley present such a capacity and are compatible with the characteristics obtained for magnitude and distance of the control earthquake. The results of this study were used to develop the Seismic Design Guidelines for Bridges of Costa Rica (CFIA, 2013).

A recent regional study was undertaken by Salgado-Galvez et al. (2022), who slightly modified the seismic zonation of Alvarado et al. (2017) and produced a seismic hazard map for the Caribbean and Central America based on a stochastic event approach. These authors considered probabilistic estimations of earthquake losses at national scale, which are used as triggers for underpinning parametric earthquake insurance. This latter regional study provides an interesting approach, although mainly for practical purposes and for insurance companies.

The most recent probabilistic seismic hazard study for Costa Rica was undertaken by Hidalgo-Leiva et al. (2023) using the seismic zonation proposed by Alvarado et al. (2017). In this study, the seismic source model parameters were updated, each seismic source was characterized, and weighted ground-motion models were used for each of the tectonic domains. These authors obtained PGA maps for a RP of 475 yrs and 2475 yrs, and subdivided the country into four seismic hazard levels: 1) extremely high for the Nicoya, Osa, and Burica peninsulas, situated directly above the subduction interplate zone (PGA 0.55–1.20 g), 2) very high for most of the Guanacaste Province in the northwestern part of the country (PGA 0.55–0.70 g), 3) high for most of the country (~41%, PGA 0.40–0.55 g) including Central Costa Rica and San José, and 4) moderate for the Talamanca Cordillera and Northern Costa Rica (PGA up to 0.40 g).

4 SEISMIC HAZARD CALCULATION

A deterministic approach was used to characterize some of the possible more critical seismic hazard scenarios in San José. The distribution of PGA linked to these scenarios was estimated according to the following steps: 1) identification of possible ruptures and magnitude of the events which could produce the highest ground motion in the city, 2) estimation of PGA distribution for rock conditions by applying selected GMPEs, 3) compilation of geotechnical and geophysical data to produce a soil condition map for the GAM, 4) estimation of PGA including the local effect, considering the soil categories given by NEHRP (2020). The following two sections describe these four steps.

4.1. DEFINITION OF THE CRITICAL RUPTURE SCENARIOS

Three critical scenarios were selected as being those which possibly pose the greatest hazard to the CCSJ according to magnitudes calculated using the scaling relationships from Stirling et al. (2002). This scaling relationship offers a magnitude-length and magnitude-area relation, developed to compare pre-instrumental and instrumental events using ordinary least squares regression. The authors used data from 389 worldwide earthquakes with magnitudes between Mw 4.6 and 8.7 (Stirling et al., 2002), complementing the dataset compiled by Wells and Coppersmith (1994). Moreover, it fulfills the criteria suggested by Stirling et al. (2013) for the selection of earthquake magnitude scaling relationships in seismic hazard assessments, based on peer-reviewed publication, tectonic relevance, global usage, and recent data (preferably less than 30 years old).

The scenarios correspond to ruptures in the Belo Horizonte-Patalillo, Río Azul and Cipreses faults, the locations of which can be seen in Figure 3. Based on these scenarios, we used a deterministic approach to characterize the soil acceleration associated with these three ruptures. The rupture lengths were estimated from fault traces reported by Montero et al. (2005) for the Belo Horizonte-Patalillo and Río Azul faults and by Rodríguez et al. (2019) for the Cipreses Fault. A revised version of the mapped fault traces for the Belo Horizonte-Patalillo and Río Azul faults was developed by Montero et al. (2016). The proposed rupture area for the Belo Horizonte-Patalillo Fault presents a dip angle of 30° to the southwest along a fault plane extending 7 km along the dip. Although the Belo Horizonte-Patalillo Fault is seismically active (Montero et al., 2005), the seismicity shows significant dispersion. We believe the Belo Horizonte-Patalillo fault plane thrusts under the western side of the Cerros de

Escazú and is limited to the west by its regional divide (see divide and epicenter in Fig. 3). The estimated dip angle is typical of thrust faults. The rupture area for the Río Azul Fault is calculated for a vertical fault plane extending from the surface to a depth of 15 km. The Río Azul shows a linear trace crossing different topographic features. Typical depths of the shallow crustal earthquakes in the Central Valley are between 0 and 15 km. The rupture area for the Cipreses Fault is estimated according to the model proposed by Rodríguez et al. (2019) for a fault plane dipping 25° to the east and down-dip 9.2 km from the surface trace. The dextral strike-slip Lara Fault limits the eastern border of the Cipreses rupture area. The rupture lengths, rupture areas, and dip angles of the three seismic scenarios are included in Table 1. The estimated magnitudes of the critical scenarios were Mw 6.2 for Belo Horizonte, Mw 6.6 for Río Azul, and Mw 6.3 for the Cipreses fault.

Although our main interest is focused on the CCSJ for the purposes of risk assessment, the hazard scenarios associated with the three critical ruptures have been produced for the entire GAM, taking advantage of the existence of microzonation data for that area, particularly given that there are also populations which, despite having lower exposure levels than San José could also be seriously affected.

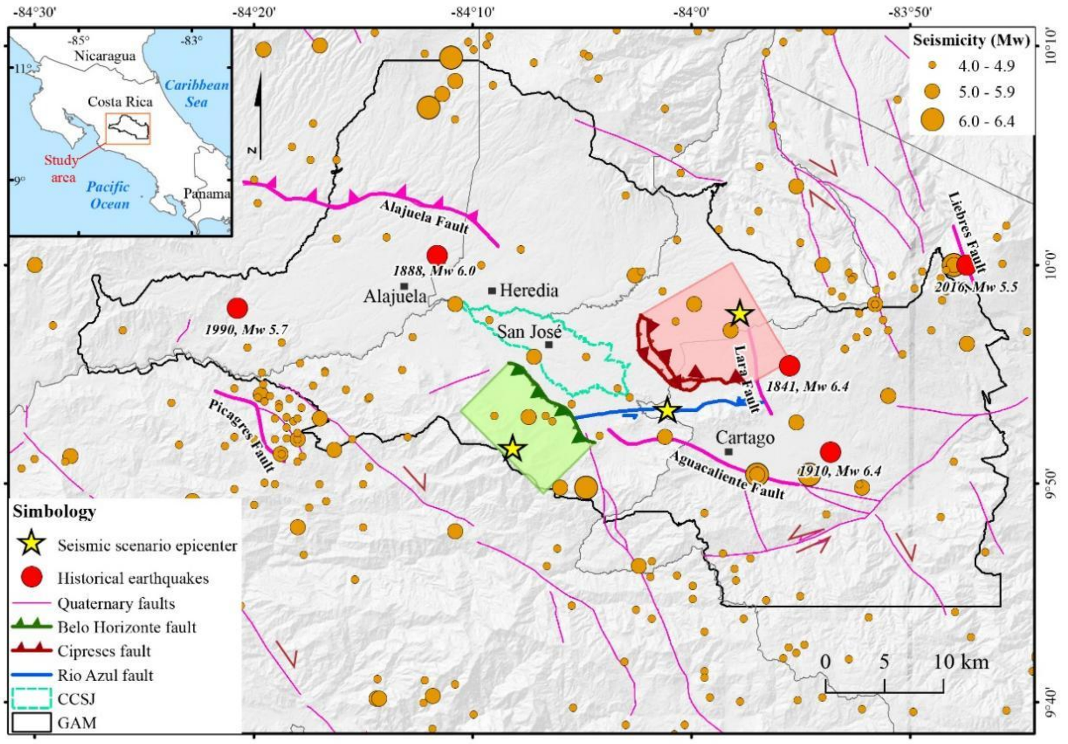

Figure 3. Seismic sources considered for seismic risk assessment in the Central Canton of San José (CCSJ). The fault rupture planes for the scenarios are represented by shaded colors. The traces of the Quaternary faults are represented in magenta and are taken from the Costa Rica Tectonic Atlas (Denyer et al., 2003). The faults associated with the historical earthquakes presented in section 3.1 are highlighted and labeled. The seismicity corresponds to shallow earthquakes (< 30 km) from the National Seismological Network earthquake catalog (RSN, 2021).

4.1.1. Belo Horizonte-Patalillo fault

The Belo Horizonte- fault is the most hazardous active fault on the western and southwestern sides of the metropolitan area of San José (Fig. 3) and has the potential to generate earthquakes of up to Mw 6.2. Based on observed previous earthquakes and by forecasting the possible ground accelerations related to this scenario regarding the magnitude and distance from San José (< 5 km), this fault is considered to be one of the most hazardous to San José.

The scenario associated with the Belo Horizonte fault corresponds to a reverse/thrust fault with a sinistral component. Tectonically, this fault is a transpressive relay between the Aguacaliente-Río Azul faults to the east and the Salitral fault to the west (Montero et al., 2005). The estimated surface rupture length would be 12.6 km (Fig. 3; Table 1), and the rupture area has a mean dip of 30°. The horizontal projection of the fault is shown in green in Figure 3. Regarding the dip angle of this fault, Montero et al. (2005) present a seismic belt with most of the events located on the southwestern side of the Belo Horizonte fault, with some showing reverse and strike-slip focal mechanisms. Hence, as regards our fault rupture scenario in the case of the Belo Horizonte fault, we estimate a dip angle of 30° to S45°W, which is perpendicular to the average strike of the fault trace of N45°W.

4.1.2. Cipreses fault

The Cipreses fault is the most hazardous active structure on the eastern side of the metropolitan area of San José (Fig. 3). It is the closest fault to this side of the city and according to its estimated rupture length and rupture area, has the potential to generate earthquakes of up to Mw 6.3. Rodríguez et al. (2019) discuss the uncertainty of the Cipreses fault seismic potential. They postulate an increase of 10% to the total length of the fault when the magnitude is estimated from empirical relationships. They concluded that the seismic potential of the Cipreses fault varies from 5.9 to 6.5. The fault trace was simplified for the purposes of this study and two fault branches were identified in the case of the Cipreses fault, known as Cipreses and Guayabos. For the rupture scenario postulated in this study, our surface rupture follows the contour of the Guayabos fault, the latter being the external trace of the Cipreses fault, which indicates that the most prominent morphotectonic signature is in the central and eastern sectors.

In the postulated scenario, the surface rupture length is 13.4 km (Fig. 3). The fault rupture area has a northeasterly trend, perpendicular to the fault trace in its northern and southern sectors. The northeastern limit of the rupture zone passes slightly west of the Lara dextral fault (Montero, 2001). The horizontal projection of the rupture area is shown in red in Figure 3. The length and area increases suggested by Rodríguez et al. (2019) are not taken into consideration. Regarding the dip angle, Rodríguez et al. (2019) identified a reverse focal mechanism for an earthquake of Mw 4.1, probably occurring along the nodal plane with a dip angle of 35° to N30°E. Their proposed tectonic fault model shows a propagation fault with sub-horizontal detachment zones and ramps. Our proposed simplified model considers a dip angle of 25° to N60°W and a maximum rupture depth of about 5 km from the surface.

4.1.3. Río Azul fault

The Río Azul fault is the most hazardous active structure located to the southern side of the metropolitan area of San José (Fig. 3). It is the closest fault to that side of the city and has the potential to generate earthquakes of up to Mw 6.6.

The Río Azul fault is an ENE sinistral strike-slip fault. To simplify the rupture model, a vertical fault plane is considered (Montero et al., 2005, 2016). The rupture model scenario proposed for this fault considers a rupture of the ground surface along the trace shown in Figure 3. The surface rupture length would be 15.4 km, and the fault rupture width would be 10 km.

4.2. GROUND MOTION SIMULATION FOR THE THREE SCENARIOS

4.2.1. GMPEs selection and rock condition calculations

The ground motion characterization for a given seismic scenario requires the inclusion of the three effects involved: the source, the path, and the site. In a deterministic study, the source effect is given by the magnitude of the considered seismic event and other available data such as the kinematics and geometry of the fault and rupture. The path effect considers the wave attenuation from the source to a given site and is usually included in the analysis through the GMPEs. The site effect addresses the wave amplification due to the local geology and topography, usually given by a coefficient intended to represent the effect of the soil conditions on the seismic waves. With regard to this latter effect, in our approach we first estimated the ground motion for rock conditions (considering vs30 = 800 m/s, as defined in the Costa Rican building code (CFIA 2003), where S1 is classified as a rock or dense soil profile with properties similar to rock and a shear-wave velocity (Vs) of 760 m/s or higher), in terms of maximum acceleration (PGA) and then we included the local effect. Finally, the response spectra were also estimated at certain points in the city of San José.

The GAM is composed of Miocene marine and continental sedimentary rocks, often influenced by volcanism. From the Miocene to the present, numerous volcanic deposits have also been emplaced, including lava flows, pyroclastic flows, and ash fall deposits, accompanied by Pliocene intrusive events and the generation of metamorphism in sedimentary rocks. Additionally, there are significant Quaternary alluvial-colluvial deposits in the transitional zone between the mountains to the south and southwest and the gently rolling relief to the north-northwest, center, and northeast. It is worthy of note that the central part of the Metropolitan Area lies entirely on lahars and thick ash deposits (Denyer and Alvarado, 2007; Schmidt et al., 2005).

The selection of a suitable GMPE is key to obtaining realistic results for each seismic scenario. The ideal situation would be to have local model availability, these being inferred from regression analysis of strong motion data recorded in the study zone. In our case, some models have been developed for the region (Climent et al., 1994; Schmidt et al., 1997), but these are only defined for prediction of PGA and a few spectral acceleration values. These models are not suitable for predicting the entire response spectra; therefore, they may not be suitable for calibrating the design spectra of the seismic code.

We used the GMPEs recommended by Hidalgo-Leiva et al (2023) for upper-plate. From international literature available in OpenQuake (GEM, 2020), these authors compiled ~150 GMPEs applicable to the tectonic context of Costa Rica and applied the exclusion criteria of Cotton et al (2006) to eliminate some of them. Using the Costa Rica data base of earthquake strong motion records and the remaining GMPEs, Hidalgo-Leiva et al. (2023) analyzed the data fit using three methods: residual calculation, likelihood model, and logarithmic likelihood model, to obtain a classification into four categories: A, B, C, and D for the models by spectral ordinate and for each tectonic regime, following the criteria proposed by Scherbaum et al. (2004).

In the present study we performed seismic hazard calculations for PGA and several spectral ordinates. Based on these calculations, the models selected were those of Cauzzi et al. (2015); Kanno et al. (2006), and Boore et al. (2014), abbreviated as CA14, KA06 and BO14, respectively. The applicability ranges and characteristics of these data sets regarding ranges in magnitude, distance and spectral periods are given in Table 2. The resulting accelerations in rock using each of these models for each proposed rupture scenario are shown in Figure 4, where the mean PGA values for each GMPE are represented.

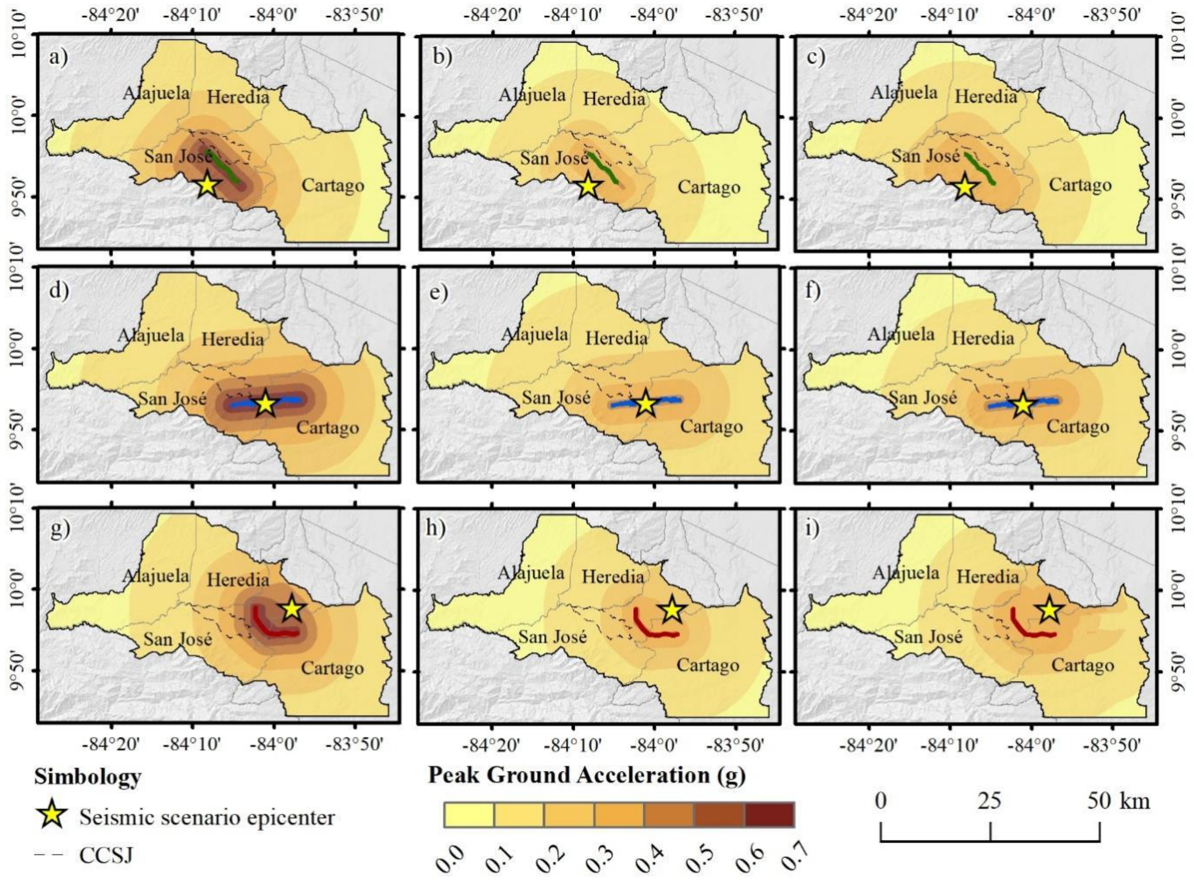

Figure 4. Expected ground motion estimated for the three defined scenarios using the three selected GMPEs for the GAM of Costa Rica: Belo Horizonte fault (a, b and c); Río Azul faults (d, e, f) and Cipreses fault (g, h, i). For each scenario, the first map is estimated with CA14 (a, d and g), the second with KA06 (b, e and h) and the third with BO14 (c, f, i).

4.2.2. Site effect and local amplification factors

We propose a seismic soil zonation for the GAM with two different levels of resolution (Fig. 5). The higher resolution corresponds to the CCSJ and its surroundings (Z1), while the lower resolution applies to the rest of the GAM (Z2). This map is based on the collection and analysis of comprehensive geological, geotechnical, geophysical, and geomorphological information.

The geological information includes the geological map by Denyer and Arias (1991). The geotechnical information is derived from the map of unconsolidated material thickness in the Metropolitan Area of San José, developed by Climent and Bolaños (1999) and published in Schmidt et al. (2005), as well as the proposed geotechnical zoning map for the Metropolitan Area (Bogantes, 1999) also in Schmidt et al. (2005).

The geophysical data, obtained mostly from Schmidt et al. (2005), includes Vs models for 7 sites within the Metropolitan Area from Spectral Analysis of Surface Waves (SASW) tests; Vs models up to 30 m depth obtained from seismic refraction tests for 8 sites within the Metropolitan Area; the fundamental soil period map (Guzmán, 1999); the isoperiod map for the Metropolitan Area of San José (Schmidt et al., 2005); and fundamental soil period values obtained using the Nakamura technique with ambient noise at 185 sites within the CCSJ (Schmidt and Esquivel-Salas, 2023). Additionally, shear wave velocity values at 30 m depth (Vs30) at 42 sites within the GAM (Schmidt et al., 2005; Schmidt 2014; IIG Consultants, 2017; IIG Consultants, 2020) are included, as detailed in Table 3. Furthermore, we took into consideration the research undertaken by Schmidt et al. (2005) on the seismic microzonation of San José to complement our research. Finally, the geomorphological information is based on the topography of the area obtained from a 10 m resolution Digital Elevation Model (DEM).

The more detailed zone corresponds to the metropolitan area of San José city and surroundings (Z1, Fig. 5), taking the map of unconsolidated material thickness (Climent and Bolaños, 1999) as a reference. A thickness-soil type relationship was identified (Fig. 5) and this was adjusted with data from 22 sites with observed Vs30 measurements[1], which helped to refine the detail and corroborate the association between the thickness ranges and the NEHRP (2020) soil-type categories. This classification was also verified through the fundamental soil period values, measured using the Nakamura technique, for 185 points within the city of San José (Schmidt-Díaz & Esquivel-Salas, 2023). It was observed that points with higher velocities coincided with areas of lower thickness, while points with lower velocities aligned with thicker areas. This pattern was also observed for intermediate velocities and thicknesses. Based on this result, a classification of soil classes for the CCSJ and its surroundings (Z1) is proposed, using the thickness contours from the Climent and Bolaños (1999) map as boundaries for each soil class. The criteria adopted are shown in Fig. 5.

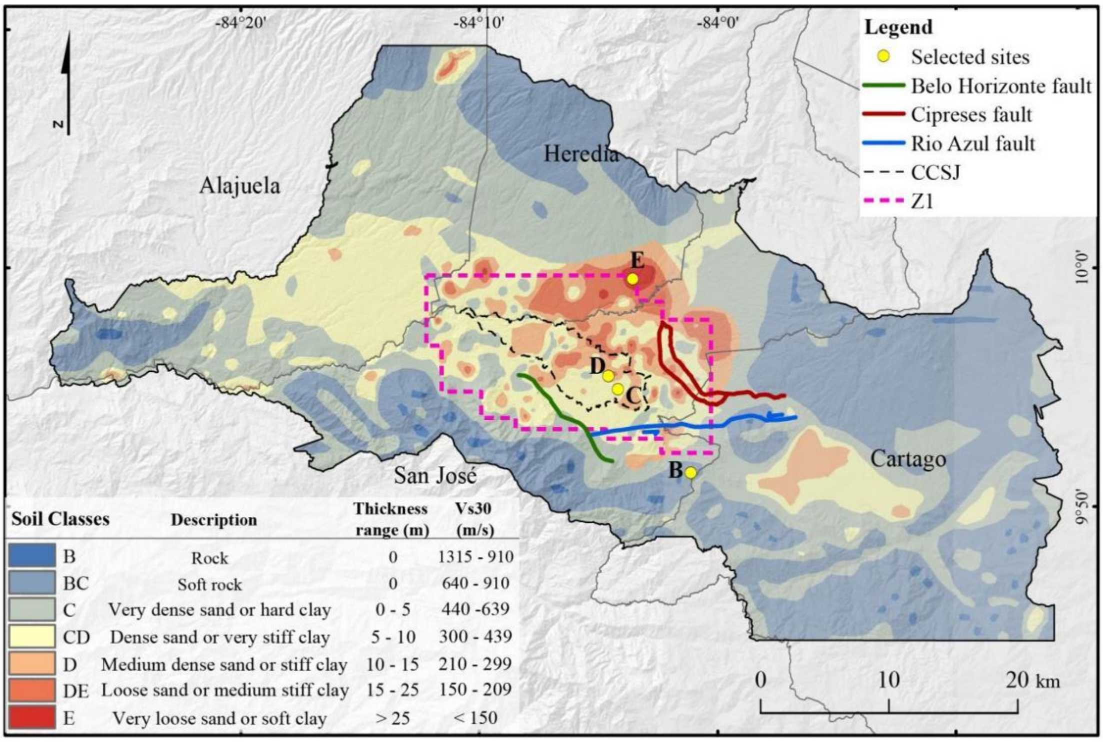

Soil Classes		Description	Thickness range (m)	Vs30 (m/s)
🟦	B	Rock	0	1315 - 910
🟦	BC	Soft rock	0	640 - 910
▨	C	Very dense sand or hard clay	0 - 5	440 -639
🟨	CD	Dense sand or very stiff clay	5 - 10	300 - 439
🟧	D	Medium dense sand or stiff clay	10 - 15	210 - 299
🟧	DE	Loose sand or medium stiff clay	15 - 25	150 - 209
🟥	E	Very loose sand or soft clay	> 25	< 150

Figure 5. Soil condition map (site effects) of the GAM, and local faults considered as critical seismic scenarios in the seismic hazard of the CCSJ. The area enclosed by the pink dashed line represents zone Z1, and the points are the sites selected for the response spectra examples. The table contains the adopted soil classification, with the thickness-type of soil based on criteria of Climent and Bolaños (1999) and the Vs30 ranges for each class according to NEHRP (2020).

---

[1] Supplementary material includes a graph showing the relationship between the Vs30 values of the evaluated sites and the soft soil thicknesses based on the Climent and Bolaños (1999) map, along with the 95% confidence interval.

No detailed information was available for the rest of the GAM (Z2) regarding the thickness of unconsolidated soils and recent sediments; hence the global mosaic Vs30 of the USGS was used (Heath et al., 2020). In this regard, it is important to clarify that not all integrated regional models rely solely on slope information. Some regional models may incorporate a variety of additional factors, such as geological data, geomorphological classification, etc. (e.g., Matsuoka et al., 2006). This mosaic is based on custom integrated topographic slope maps (Heath et al. 2020), and in the case of the GAM, the Vs30 values range between 208 and 900 m/s, and are classified as type B, CB, C, CD, D and DE soils, according to the NEHRP (2020). In specific areas of Z2, the soil classification obtained was correlated with Vs30 measurements at the remaining 20 points with known Vs30 values (Table 3). Seven of these sites were located at different points across the GAM, seven in Cartago (east of the GAM) and the remaining six on the Inter-American highway, between San Ramón-San José (west of the GAM). Finally, the soil categories map integrating the highest resolution zone (Z1) and the rest of the GAM (Z2) was determined through a detailed review of the transition zones, prioritizing the information from Z1. Hence, when the soil classification between Z1 and Z2 did not coincide, the information from Z1 was used and the contours in these areas were smoothed according to the geomorphological characteristics.

Once the soil condition map had been defined according to the NEHRP 2020 soil classes, amplification factors were assigned to each of them (Table 4). Spectral amplification factors determined by Mixco (2021a y 2021b) for El Salvador were used, assuming geological and tectonic conditions which are similar to the predominant volcanic soils found in Costa Rica. Through a comprehensive evaluation of dynamic soil characterization of representative soils in El Salvador, Mixco (2021a y 2021b) determined amplification factors for 22 levels of spectral acceleration, 14 structural periods, and 6 soil classes (BC, C, CD, D, DE, and E) using empirical and analytical methods.

More specifically, Mixco (2021a y 2021b) used accelerometer records for El Salvador and three different techniques to obtain empirical amplification factors: spectral ratios with respect to a reference site (SSR), spectral ratios of seismic records (HVSR), and optimal selection of attenuation models followed by deconvolution. The analytical-theoretical amplification functions for each soil class were obtained using a linear-equivalent approach of 1D simulations, generating multiple stochastic profiles through Monte Carlo simulations. This involved varying dynamic properties (Vs, G/Gmax curves, hysteretic damping curves) and thicknesses, utilizing geological and geotechnical information from 16 exploration wells, with direct knowledge of their Vs structure and stratigraphy, subjected to different earthquakes with varying intensity levels.

The final amplification factors resulted from averaging those obtained through empirical techniques with those from simulations. We consider that these amplification factors, carefully estimated for soils from El Salvador, are those that can most accurately reflect the amplification of the considered soil categories, which are also those that exist in Costa Rica.

4.2.3. Final maps and response spectra calculation

For the calculation of the final maps and response spectra, a logic tree was constructed with a node representing the attenuation, incorporating the weights proposed by Hidalgo Leiva et al. (2023) for the three selected models. These weights were proposed as results of an analysis based on the goodness-of-fit to the local data. The models developed by Cauzzi et al. (2015) and Kanno et al (2006) were weighted with the same factor of 0.4, while Boore et al (2014) was weighted with 0.2 as the fit was worse than that of the other models. The PGA maps resulting from the application of the logic tree presenting the rock conditions for the three scenarios are represented in Figures 6a, 6c, and 6e.

From the analysis of the maps, including the local effect, it was determined that the most hazardous scenario was that of Río Azul, which would generate PGA ~ 0.65 g in some areas to the south of the CCSJ and up to 0.75 g in other areas of the GAM. The Cipreses scenario presents accelerations of less than 0.5 g within the CCSJ, but in some areas of the GAM and to the NE of San José city, the PGA would reach values of 0.8 g. The Belo Horizonte scenario would have a greater impact to the southeast of the metropolitan area, reaching PGA values of 0.5 g in the CCSJ and presenting the greatest accelerations to the SW of the GAM, at around 0.6 g.

The rock acceleration values for the three defined scenarios were superimposed over the soil classification map (Fig. 5), and by applying the spectral amplification factors (Table 4) the PGA maps were obtained, including the local effect in the CCSJ and the GAM (Fig. 6b, 6d, and 6f). The short period (0.2 s) and long period (1 s) spectral acceleration resulting from the DSHA analysis for the three scenarios have also been simulated with the same logic tree scheme as that used for the PGA calculation. In this case, the maps of SA (0.2 s) and SA (1 s) are represented for the three scenarios incorporating the local effect (Fig. 7).

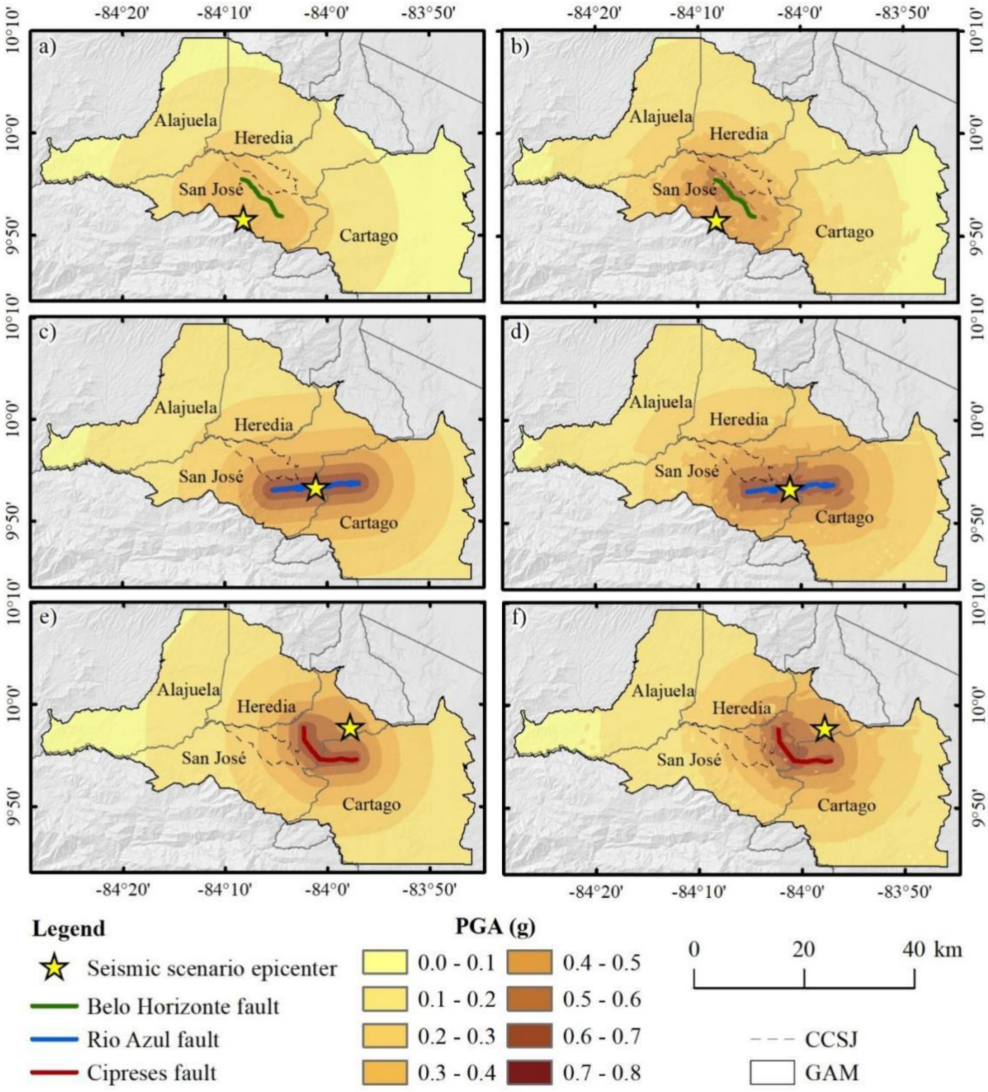

Figure 6. Expected ground motion maps for PGA mean values using the weight scheme of the considered logic tree for each critical scenario: (a) Belo Horizonte in rock ; (b) Belo Horizonte including local site effects; (c) Río Azul in rock; (d) Rio Azul including local site effects; (e) Cipreses in rock; (f) Cipreses including local site effects .

The response spectra were also estimated for four sites within the metropolitan area of San José. The sites were chosen considering the variability of soil classes and distances to each of the faults, so that each site corresponds to a soil class and different distances to the rupture scenarios. These were compared with those for similar soils in the seismic Code of Costa Rica (CSCR14), and the results for the three scenarios are shown in Figure 8. The spectra represented correspond to the mean values μ of SA(T) obtained by applying the GMPEs in each scenario, combined according to the logic tree scheme considered in the PSHA and to the values obtained considering the standard deviation of each model ($\mu \pm \sigma$) .

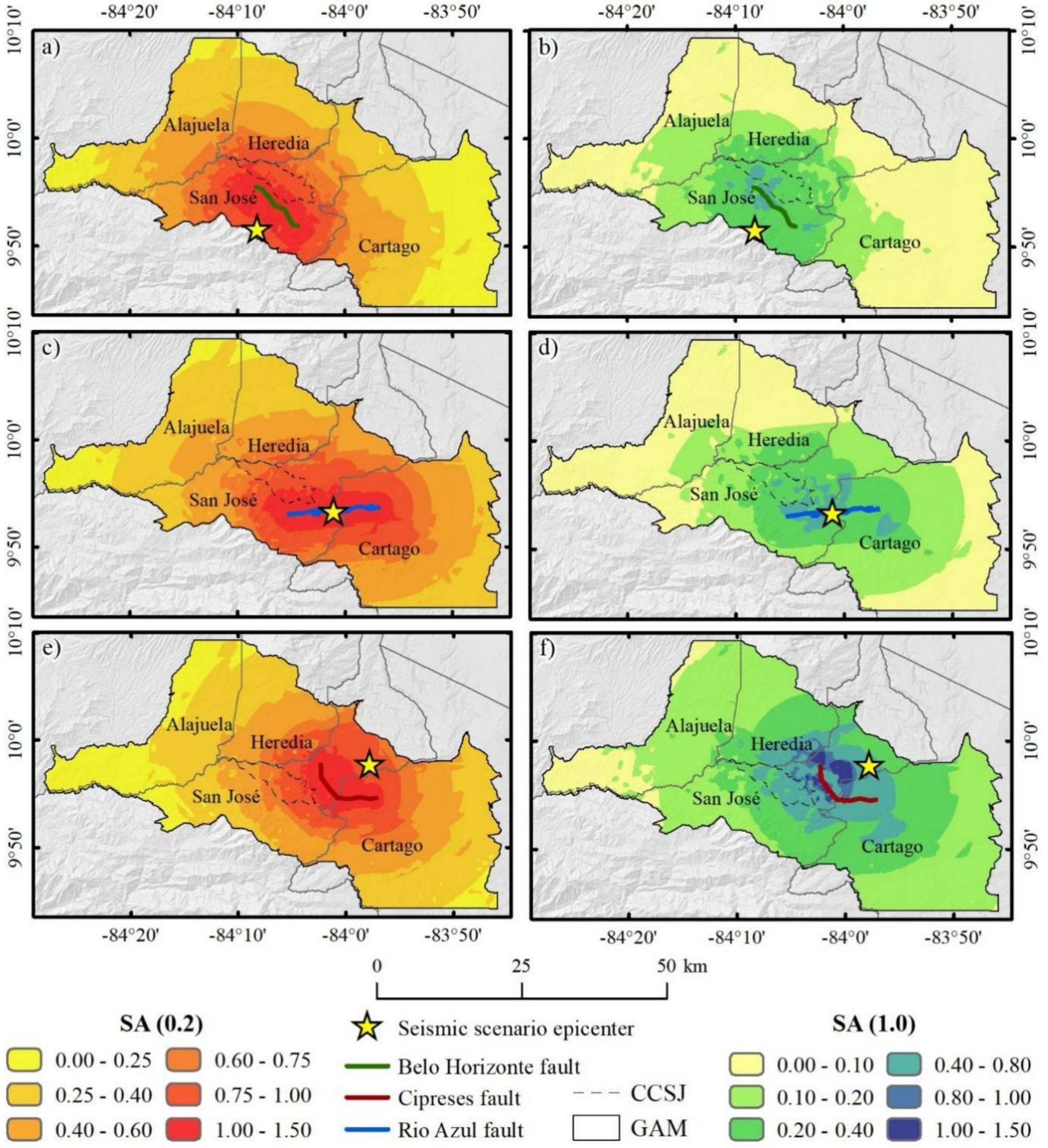

Figure 7. Expected ground motion including local site effects using the weight scheme of the logic tree for the scenario in the Belo Horizonte fault a) SA (0.2 s) and b) SA (1.0 s.); the scenario in Río Azul fault c) SA (0.2 s.) and d) SA (1.0 s.); the scenario in Cipreses fault e) SA (0.2 s.) and f) SA (1.0 s.).

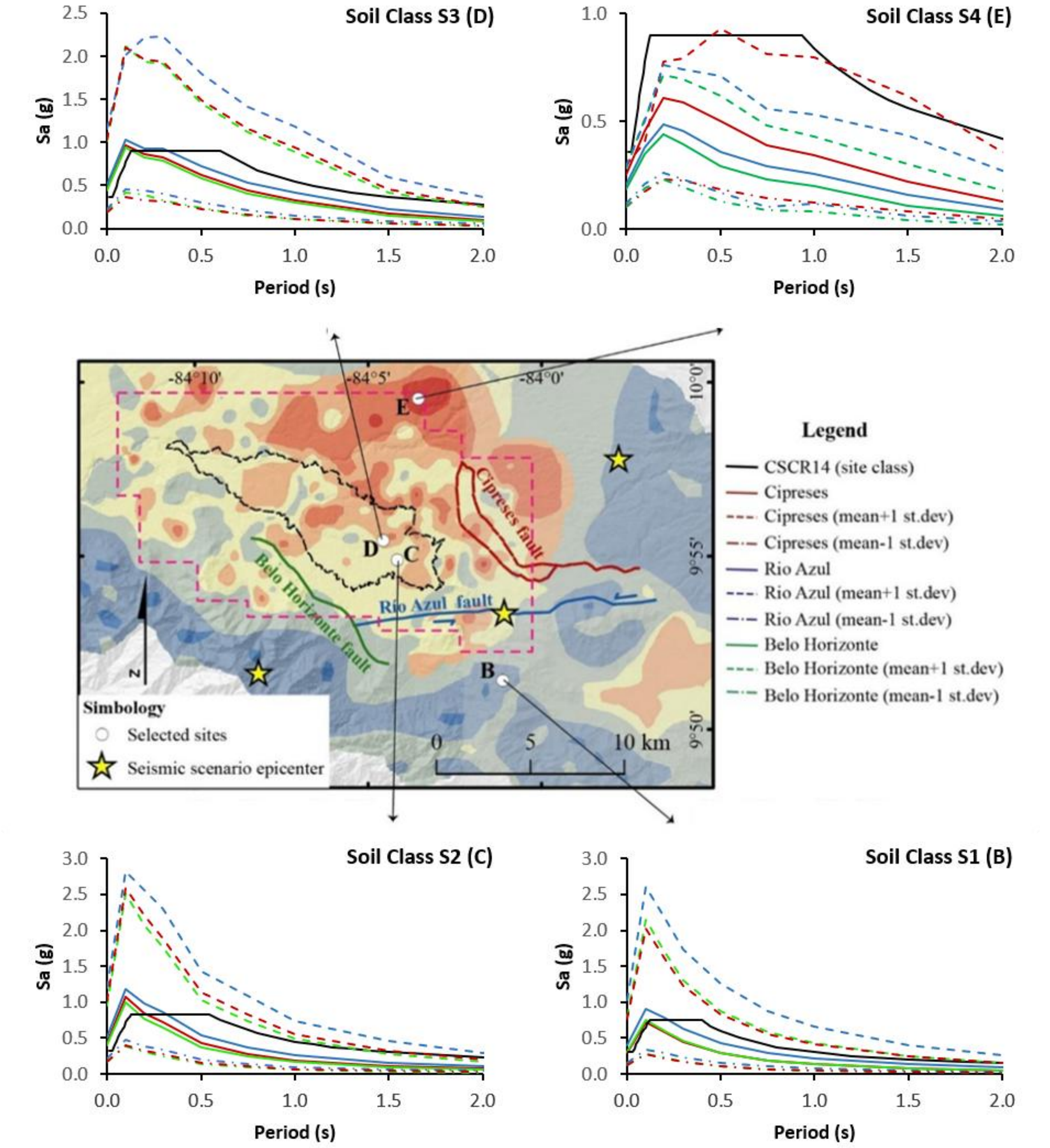

Figure 8. Comparison of site-specific acceleration response spectra at different site classes for the three simulated scenarios (the red line, green line, and blue line, correspond to the results in Cipreses, Belo Horizonte, and Río Azul, respectively) with their corresponding site class CSCR14 spectrum. The spectra represented correspond to the mean values μ of SA(T) obtained by applying the GMPEs in each scenario, and to the values obtained considering the standard deviation of each model (μ ± σ) .The soil classes correspond to the same as those indicated in Figure 5. The area enclosed by the pink dashed lines represents zone Z1 (CCSJ), and the points are the sites selected for the response spectra examples. The equivalence between the classes A, B, C and D defined by the NERHP (2020) and S1, S2, S3 and S4 is: S1~B; S2~C, S3~C, and S4~D (CFIA, 2014).

To facilitate comparison, it should be noted that the Costa Rica code defines four types of soil, termed S1, S2, S3 and S4, which are equivalent to the classes defined by the NERHP (2020): S1~B; S2~C S3 ~C and S4~D.

Among the spectra corresponding to the three rupture scenarios, the one for Río Azul is dominant over the other two, except for the point located to the NE of the study area where the Cipreses scenario dominates as it presents soil type E and is the closest to the Cipreses fault. The spectrum of the Belo Horizonte fault scenario is the lowest of all the cases considered, thus pointing to the lowest hazard. When comparing the spectra of the three scenarios with those of the Costa Rican building code, it can be observed that the latter is surpassed by the Cipreses and Río Azul spectra (mean values, μ) at the two points located farthest east, on S2 and S3 soils, for periods less than 0.3 seconds. The spectrum of the code is also exceeded by the mean spectrum of Río Azul at the point located on S1 soil for periods of less than 0.2 s.

Although more cases related to different combinations of soil type and distance to the simulated rupture scenarios can be analyzed, the results obtained lead us to question the degree of conservatism of the code. For short periods on the soils S1 (or B), S2 (or C) and S3 (or D), it can be observed that the spectrum of the code is exceeded by the mean spectrum (μ) for most of the simulated scenarious. Furthermore, the spectra obtained here, considering the standard deviation of the GMPEs ($\mu \pm \sigma$), exceed the code spectra across the entire range of periods for these three soil types.

However, the spectrum of the code is clearly dominant over the others for the entire range of periods at the point located on soil S4 (or E), both on the average spectra (μ) and ($\mu \pm \sigma$). This suggests that the code spectrum may be excessively conservative for this type of soil, potentially overestimating the seismic hazard in these conditions.

5 MT-INSAR DEFORMATION AND STRESS TENDENCY ANALYSES

5.1. DEFORMATION OF THE CENTRAL CANTON OF SAN JOSÉ (CCSJ)

To complement the study, the surface deformation patterns were characterized and evaluated through multi temporal InSAR analysis (MT-InSAR). Considering the nature of the terrain and the mixture of urbanized and vegetated land cover, the SBAS (small-baseline) approach was selected. The degree of uncertainty of SBAS processing is in the order of ~1 mm/year for velocity (Lanari et al., 2004), similar to that of Persistent Scatterers Interferometry techniques (PSI) (Crosetto et al., 2016). MT-InSAR processing was carried out in LiCSBAS: Looking inside the Continents from Space-Small Baseline Subset (Morishita et al., 2020), an open-source InSAR time series analysis package that integrates with LiCSAR (Lazecky et al, 2020; Morishita et al., 2020; González et al. 2016; Lawrence et al. 2013), developed by the Centre for Observation and Modelling of Earthquakes, Volcanoes and Tectonics (COMET) at University of Leeds. LiCSAR pre-processing allows users to save time and disk space while obtaining the results of InSAR time series analysis in the frame of JASMIN, the UK's collaborative data analysis environment (Lawrence et al., 2013). In the LiCSBAS processing scheme, interferograms with many unwrapping errors are automatically identified by loop closure and removed. Reliable time series and velocities are derived with the aid of masking using several noise indices. The straightforward implementation of atmospheric corrections to reduce noise is achieved with the Generic Atmospheric Correction Online Service for InSAR (GACOS). LiCSBAS can detect both large-scale (>100 km) and localized (~km) deformations with an accuracy of ~2 mm/yr (Morishita et al., 2020).

The extent of the study area was set to include the three local faults selected for the scenarios surrounding the target area, the CCSJ (Fig. 8). For the analysis of deformation of the CCSJ, we worked with the frames provided by COMET (2021) using the available data from Sentinel-1 A/B. The frames 092A_08036_141719 and 084D_08033_121612 include 947 (422+ 525) interferograms obtained between March 17, 2017, and January 2, 2022. Interferograms were calculated from 116 Sentinel-1 ascending images on track 92, and 137 images from the descending track 84, respectively (Morishita et al. 2020).

The reference point for the MT-InSAR analysis was selected by LICSBAS considering high coherence (>0.95) and stability along the time series and was located at the following coordinates: 9.965° (Lat) and -84.108° (Long) (WGS84). The deformation velocity data were filtered with the coherence mask generated by LiCSBAS, producing a vectorial point layer with deformation time series and velocity for each point.

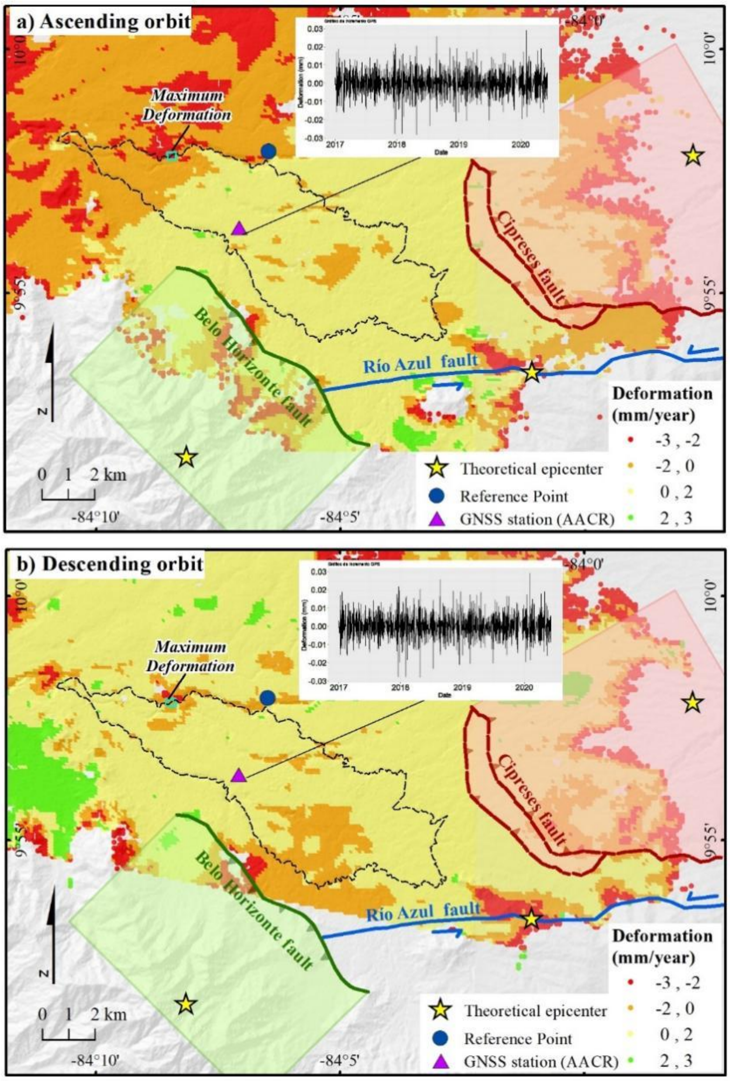

Figure 9. Deformation velocities (mm/year) in satellite line-of-sight (LOS) direction for the Central Canton of San José (2017-2022) estimated using the LiCSBAS technique in ascending (a) and descending (b) orbits. The fault rupture scenarios are represented in shaded colors.

The results show deformations in the CCSJ ranging from -2 to 2 mm/year in Line-of-sight direction (LOS) computed both for ascending and descending geometries (Table 5, Fig. 9). Results were validated with data from the GNSS station located in the study area (AACR GPS; Lat: 9.939, Long: -84.118) (Subset in the same figure as LOS velocity maps), matching the recorded velocities with a vertical displacement rate of -0.97 +/- 1.70 mm/year for the period 2012-2020 (Blewitt et al., 2018). The deformation on the three faults, the ruptures of which are identified as the critical scenarios, is small compared to that observed in the two main left-lateral faults of the Central Valley: Aguacaliente and Navarro (Fig. 3). According to Portela et al (2020), a cumulative deformation of over 1 cm/year has been estimated between the North and the South of the Aguacaliente-Navarro Fault System. The lesser deformation found in the Bello Horizonte, Cipreses and Río Azul faults could indicate that in these cases a smaller amount of energy is being released aseismically or that it is gradually accumulating, thus increasing the probability of a strong earthquake.

5.2. REACTIVATION POTENTIAL OF THE CIPRESES, RÍO AZUL AND BELO HORIZONTE FAULTS UNDER THE SAN JOSÉ TENSOR.

An additional analysis was performed to assess the slip and dilatation tendencies of the three faults in the study area. Tectonic stress is recognized as the most important factor controlling seismic activity. The parameters of this stress, represented in a stress tensor, are derived from sources such as the formal inversion of representative populations of focal mechanisms and/or fault-slip data. Fault reactivation depends on shear and normal stress, pore pressure, and frictional properties. When in situ records are unavailable, these parameters can be derived from the stress tensor and applied in conjunction with established geomechanical laws to forecast the theoretical behavior of fault planes.

Conejo and Linkimer (2021) calculated a highly representative population of 11 focal mechanisms with hypocenters between 2.6 and 9.8 km depth, located immediately to the north and northwest of the tectonic structures studied (Fig. 10).

The histogram also illustrates the distribution of the difference between the theoretical rake angle and the measured one, with an accepted value of 30° within a Gaussian distribution. The triangle classifies the kinematics of the focal mechanisms, predominantly strike-slip. The absolute magnitudes, which are necessary for calculating slip and dilation tendencies, are included as they were derived from the stress ratio $\Psi = \sigma 3/\sigma 1$, provided by the Win-Tensor program as part of the inversion process. This ratio is applied, along with the vertical load (σv) according to Angelier (1989), to determine the absolute magnitudes at a given depth for the acting stress regime. This shows a strong correlation with in situ geomechanical tests conducted in neighboring regions (Monge Sandi, 2003).

The selected population is highly representative of the focal solutions prevailing in the studied region and throughout central Costa Rica, where strike-slip mechanisms dominate over other recent regimes, including the outcropping thrusts illustrated in Figures 3 and 10. The database for focal mechanisms covering the period from 1924 to 2021 (López and Carvajal, 2024) confirms this observation, and calculations with other events yield a similar stress tensor for the entire region.

By inverting their nodal planes using the Win-Tensor free software (Delvaux and Sperner, 2003), a highly reliable tectonic stress tensor was determined, which effectively explains and accommodates the kinematics of all the faults. This tensor received a quality rating of A, the highest level according to the World Stress Map quality scheme. The results, presented in Figure 10, are consistent with those of López (2012) on a regional scale using larger datasets.

This tensor, which we refer to as the San José tensor, was applied to the traces of the structures identified at that depth to model their behavior regarding the normalized slip tendency of a surface, defined by the ratio of shear stress to normal stress on that surface ($Ts= \sigma n/\tau s$ (max)) (Morris et al., 1996). Additionally, we calculated the dilatation tendency, which represents the stress acting normal to a given surface, defined as $Td = (\sigma 1-\sigma n)/(\sigma 1-\sigma 3)$, (Ferril et al., 1999). Both measures are unitless and range from 0 to 1. These tendencies were implemented using the FracPaQ and FracTend MATLAB code programs for 2D and 3D analysis (Healy et al., 2017, 2022), which are widely used in the applied tectonic stress research community.

We present the results of both 2D and 3D fault reactivation potential analyses (Figs. 11 and 12). The 2D analysis revealed significant changes along the strike of the faults, especially where reorientation occurs. For the Cipreses fault, the combination of high Ts and medium to high Td in localized segments suggests potential activation in its northern and eastern sections. The proximity to the active Irazú volcano could promote hydrothermal fluid migration along these fractures, reducing friction on the fault planes and encouraging displacement.

The eastern sector of the Río Azul fault exhibits significant parallelism with the Cipreses fault, separated by only 1.5 km, and shows high Ts values with medium Td (Fig. 11). Additionally, its kinematic affinity, orientation, and relative proximity to the Aguacaliente fault (not shown) suggest a possible hydraulic connection between these structures. The postulated neotectonic activity (Alonso-Henar et al., 2013) further supports this interaction. In comparison with Cipreses, the Río Azul fault has longer continuous sectors with Ts values above 0.8, while smaller bends display medium Ts values (0.4–0.6), giving this fault a slightly higher reactivation potential. On the other hand, the Belo Horizonte fault shows Ts values below 0.65, except for one segment where it reaches 0.85, near its intersection with the Río Azul fault. This suggests that activity in the Río Azul fault could trigger seismic events in the Belo Horizonte fault. However, the low Td values indicate a relatively lower reactivation potential for Belo Horizonte overall.

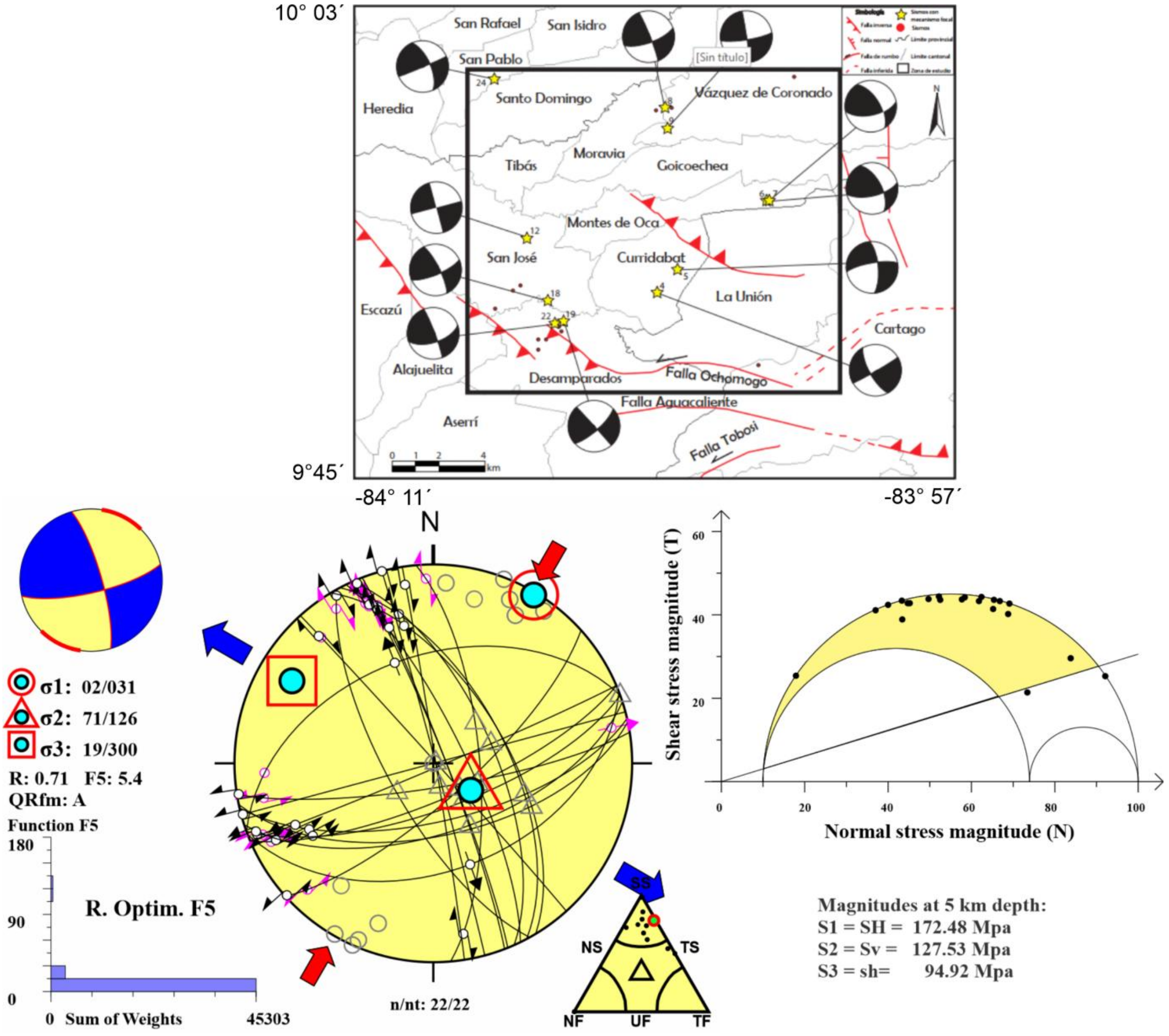

Figure 10. Location of the 11 focal mechanisms of the transcurrent regime reported by Conejo and Linkimer (2021) and the San José stress tensor of quality A, determined from the respective inversion at a depth of 5 km. Only the relative magnitudes are generated by the stress inversion method and are depicted in the 3D Mohr diagram where its friction line lies just below the fault poles ensuring its mechanical activation. σ_1, σ_2, and σ_3 are the magnitudes of the maximum, intermediate, and minimum principal stress axes of the resolved stress tensor, while R = σ_2-σ_3 / σ_1-σ_3, varying between 0 and 1, defines its shape and stability. Values around 0.5 are stable. Acronyms of the fault classification triangle: NF= Normal, TF= Thrust Fault, TS=Transpressive fault, SS= Strike-Slip Fault, NS= Transtensive Fault, UF= Unknown Fault (WSM criteria). The units of σ_1, σ_2, and σ_3 are MPa.

Consequently, from the 2D analysis, the Río Azul fault appears to have the highest reactivation potential in terms of Ts, followed by Cipreses, especially in its northern branch where Td values between 0.6 and 1.0 coincide spatially with high Ts (Fig. 11).

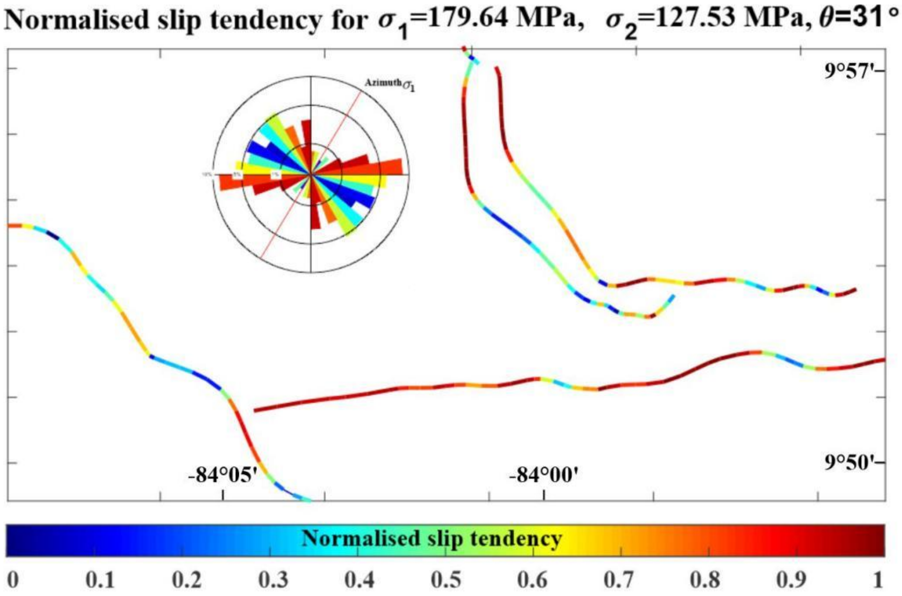
Normalised slip tendency for σ_1=179.64 MPa, σ_2=127.53 MPa, θ=31°

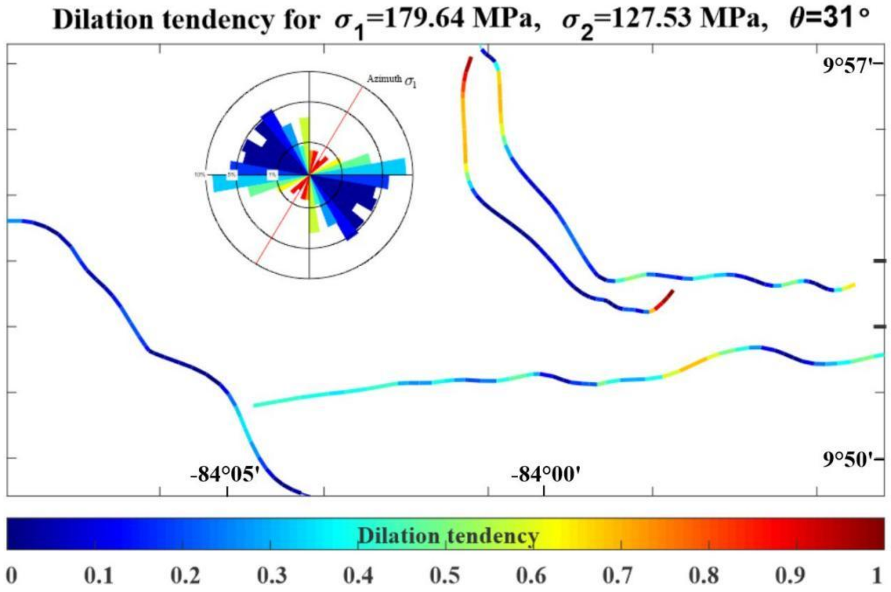
Dilation tendency for σ_1=179.64 MPa, σ_2=127.53 MPa, θ=31°

Figure 11. Map view illustrating the behavior scenarios of the Ts and Td fault traces at a depth of 5 km. The rose diagrams display the orientation and magnitude of each segment based on their Ts and Td values. θ represents the azimuth of σ_1. Notice the contrasting changes along the strike, generally showing medium to high Td and Ts within 10°-45° of the θ orientation, except the Belo Horizonte fault, which align well with the ongoing strike-slip tectonics.

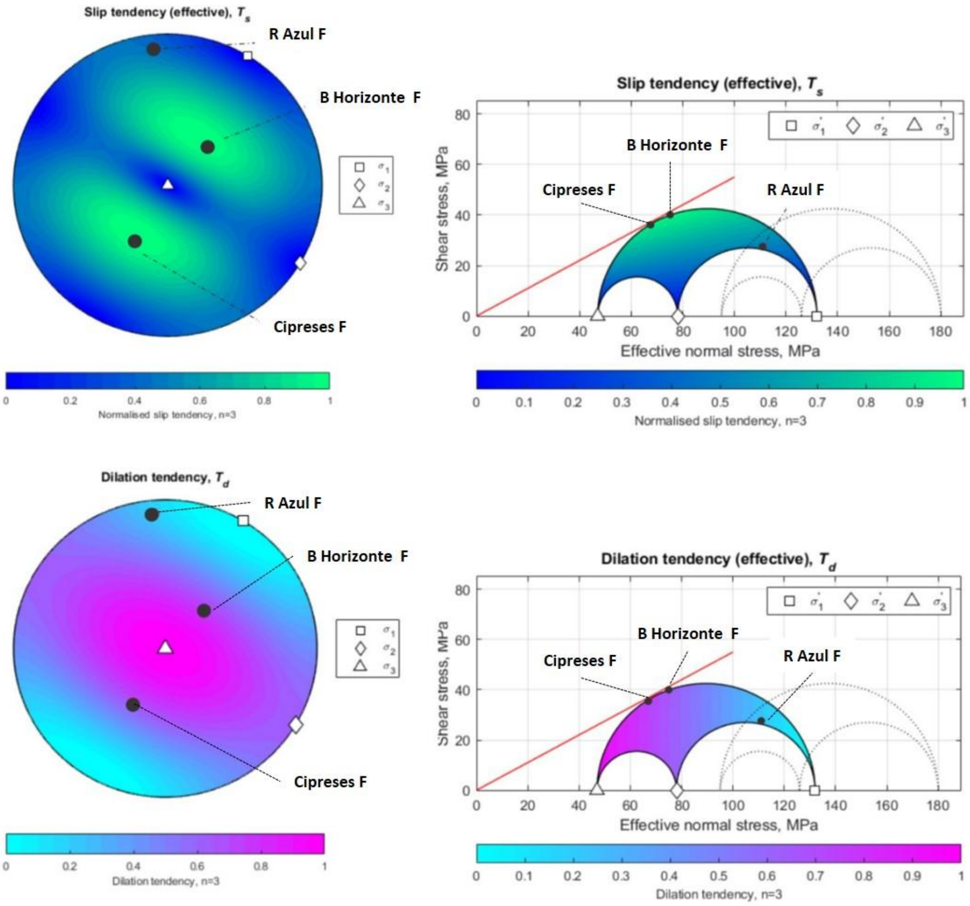

Figure 12. On the left, the figure shows two stereograms representing the slip tendency Ts (up) and dilatation tendency (down). In the upper stereogram, the color scale below the diagram ranges from blue (low slip tendency) to green (high slip tendency). In the lower stereogram, the color mapping goes from blue (low dilation tendency) to magenta (high dilation tendency). The poles of the three studied system faults, Cipreses, Belo Horizonte, and Río Azul, are represented (black points), in both stereograms. On the right, the figure shows the 3D Mohr diagram, which plots shear stress on the y-axis against effective normal stress on the x-axis, both for slip tendency (up) and dilatation tendency (down). The red line indicates a failure envelope or friction criterion, beyond which slip might occur. The diagram includes the three normal stress components: σ_1, σ_2, σ_3. The faults are positioned according to their effective normal and shear stress values. The color gradient shows values of the slip and dilatation tendency in a similar way to the stereograms (left figures.)

The 3D analysis provides further insight into the behavior of Ts and Td, focusing on the mechanical reactivation of the faults. Figure 12 shows stereograms of slip and dilatation tendencies along with Mohr diagrams, which illustrate whether the faults are positioned in favorable conditions based on normal and shear stress values. The Cipreses and Belo Horizonte faults show the highest Ts (1.0) and Td (0.75) values, positioning them in favorable orientations for reactivation. In contrast, the Río Azul fault displays Ts and Td values below 0.3, placing it in the least favorable orientation according to the 3D Mohr diagram.

In summary, the 2D analysis suggests that the Río Azul and Cipreses faults have the highest reactivation potential, while the 3D analysis indicates that the Cipreses and Belo Horizonte faults are better oriented for reactivation. Despite these differences, integrating the 2D and 3D results shows that all three faults exhibit a notable potential for reactivation.

It is important to note that the 3D model assumes a constant dip and strike for each fault plane, while the 2D model accounts for both gentle and sharp bends along the faults. This gives the 2D analysis a more realistic and detailed representation of the faults' tectonic behavior.

6 SUMMARY, DISCUSSION AND FINAL REMARKS

The city of San José is surrounded by several complex fault systems and has been affected by numerous destructive earthquakes throughout its history. Bearing in mind the high seismogenic potential of these fault along with the elevated degree of vulnerability, the high seismic risk to which the capital of the country is exposed can be affirmed. This fact underlies the present study, the main objective of which was to analyze and characterize the critical scenarios that could be generated in San José, identifying some of the most important local faults and their maximum magnitudes, as well as simulating the corresponding expected ground motions using a deterministic approach.

To estimate the local effects on the expected ground motion, we proposed a soil categories map that aligns with other related studies (Denyer and Arias, 1991; Climent and Bolaños, 1999; Bogantes, 1999; Guzmán, 1999; Schmidt et al., 2005; Schmidt, 2014; IIG Consultants, 2017; IIG Consultants, 2020; Schmidt and Esquivel-Salas, 2023).

The soil conditions map proposed in this study indicates that the soils in the GAM correspond to six types: B, CB, C, CD, D, and DE, according to the NEHRP (2020) classification. The Vs30 values in these areas range between 208 and 900 m/s, and the thickness of unconsolidated material varies from 5 m to more than 25 m (Fig. 5).

The critical scenarios identified correspond to ruptures in the Bello Horizonte, Cipreses, and Río Azul faults, where possible earthquakes of Mw 6.2, 6.3 and 6.6, respectively, could occur. The expected ground motion linked to these scenarios was firstly estimated for rock conditions and secondly, local effects in the expected ground motion were included. In the GAM, near the trace of the faults, the maximum PGA values obtained in our study were 0.6 g for the scenario of Río Azul and 0.5 g for the other two scenarios (for rock conditions) although within the CCSJ the PGA would not exceed a value of 0.5 g under any of the scenarios (Figs. 6a, 6c, and 6e).

Our study is deterministic and therefore we do not estimate probabilities for the accelerations found, however we observe that these accelerations are of the same order as those estimated in previous probabilistic studies for a return period of 500 years (Rojas et al, 1998; Fernández and Rojas, 2000; Benito et al., 2012). The accelerations simulated in this research for the three deterministic scenarios in the country's capital, ranging from 0.4 and 0.5 g on rock sites, correspond to those previously estimated in probabilistic studies with a 10% probability of exceeding this in 50 years.

Furthermore, in the RESIS II project, a control earthquake in San José was determined for a return period of 500 years, through disaggregation of the hazard from the results of a probabilistic study. Taking the PGA and SA(1s) as target motion, a control earthquake given by (Mw 6.5-6.7; Rrup 0-15 km) may be assumed for the short and long period motion. In any case, the tectonic regime that contributes most to hazard in CCSJ is local faulting and not subduction. In summary, the three simulated scenarios in our study are compatible with that control earthquake and represent a significant contribution to the hazard for a return period of 500 years. However, in RESIS II, the specific fault capable of generating the control earthquake were not identified. An added value of the work presented here is that we have defined specific scenarios of rupture in faults with known focal mechanisms, which allows more accurate simulations not only of the PGA, but also of the response spectrum. Thus, the fact that the magnitude-distance pair (Mw, R) estimated in RESIS II for PR 500 years is compatible with the assumed ruptures in the faults proximate to the CCSJ allows us to form an idea of the probability associated with the scenarios proposed here.

By including the local effect in the estimation of movement, PGA values of ~ 0.8 g are reached in some GAM areas for the Cipreses and Río Azul scenarios, with the Belo Horizonte scenario being less critical, where PGA values not exceeding 0.6 g. In the CCSJ, the first two scenarios would generate maximum accelerations up to 0.65 g, while the third scenario would reach maximum accelerations of 0.5 g (Figs. 6b, 6d, and 6f). The spectral accelerations SA(T) have also been simulated for periods T of 0.2 and 1 s (Fig. 7), for the three rupture scenarios contemplated. For these parameters' maximum values in the CCSJ of between 0.75 and 1g for SA (0.2s) and between 0.2 and 0.4 g for SA (1 s) have been obtained.

These are strictly hazard results and do not quantify the risk that the proposed scenarios could pose in the CCSJ, since this would require a detailed characterization of vulnerability and exposure, which could be the focus of a subsequent study taking the hazard scenarios presented here as input. However, an estimate of the macroseismic intensity derived from the acceleration values obtained can give us an idea of the risk presented by the simulated hazard scenarios. Linkimer (2008) deduced a relationship between macroseismoc intensity (I_{MM}) and peak ground acceleration (PGA) from Costa Rican data, but it was only applicable for PGA < 0.3 g and I_{MM} <VII. To estimate the intensity with the acceleration ranges that we are dealing with, two valid correlations are those proposed by Murphy and O Brien (1977) and Trifunac and Brady (1975). According to both correlations, the intensity I_{MM} that would result for the less critical scenario, of Bello Horizonte would be VIII-IX in the CCSJ, while for Cipreses and Río Azul with PGA that reach 0.65 g, the intensities could be higher than IX.

The response spectra estimated for the three scenarios at four chosen points of the GAM in different types of soil were compared with those proposed by the Costa Rica Building Code (CFIA, 2013, 2014). Considering the uncertainties inherent to GMPEs, we have calculated the specific response spectra from the mean values (μ) given by the different GMPEs without considering their standard deviation (epsilon 0) and also from the mean values plus/minus the deviation ($\mu \pm \sigma$) .

Thus, the 50th, 84 th and 16 th percentiles have been represented against spectra derived from seismic codes at four points with different soils conditions (Fig. 8), evidencing that: 1) The spectrum of the Río Azul scenario is dominant over the others, except for that obtained at the point closest to Cipreses, where this scenario is dominant. The spectrum of Belo Horizonte is the lowest of all the points analyzed, 2) The spectra of the code are exceeded by those of one or several scenarios at the points located in S1, S2 and S3 soils. The mean spectra estimated here (μ) are higher than those of the code for short structural periods. When we consider one standard deviation in the GMPEs, the resulting spectra ($\mu \pm \sigma$) of the simulated scenarios exceed the code for all the periods. However, the spectrum of the code is very conservative at the point with soil S4 compared to those of the three scenarios over the entire range of periods.

Furthermore, the analysis of the deformation from radar images taken from the Sentinel 1 satellite over the last five years, identified deformation rates of between -3 mm/year (sinking) and 2 mm/year (uplifting) in the case of the GAM, and between 0 and 2 mm/year for the CCSJ (Fig. 9). This deformation is considerably less than that reported in recent estimations (1 cm/year) for two of the main left-lateral fault systems of the Central Valley, the Aguacaliente and Navarro faults (Portela et al., 2020). This seems to indicate either that the energy released aseismically in the faults of our rupture scenarios is markedly lower than other nearby major fault systems, or that there is a gradual accumulation of stress in the faults of our scenarios.

The reactivation potential of the three faults examined in this study was evaluated by calculating a tectonic stress tensor, which was applied to the fault traces at a depth of 5 km—consistent with the average depth of the hypocenters determined from the focal mechanisms used in the inversions (Figs. 10, 11, and 12). Analyses in both 2D and 3D were conducted to model the behavior of the faults, focusing on their normalized slip tendency (Ts) and dilation tendency (Td). The 2D analysis suggests that the Río Azul and Cipreses faults have the highest reactivation potential, while the 3D analysis indicates that the Cipreses and Belo Horizonte faults are better oriented for reactivation. Despite these differences, integrating the 2D and 3D results shows that all three faults exhibit a notable potential for reactivation.

The seismic history of the region, the deformation rates found, and the slip-dilation stress tendencies identified (Figs. 9, 10, 11, and 12) allow us to infer pre-stressing of the faults, revealing that the ruptures modeled, and the simulated ground motions identified in this study, may occur in the not-too-distant future. Moreover, four destructive earthquakes occurred in or near the Costa Rica Central Valley between 1841 and 1924, with a range of magnitudes between Mw 6.0 and 7.0 (Fig. 2), generating MMI of between VIII and X, and seriously affecting San José, where intensities reached VII MMI. In the last 100 years, only two earthquakes of magnitudes Mw 5.5 and 5.7 have occurred in the Central Valley of Costa Rica, causing only minor damages in the CCSJ. Given this historical data, an apparent seismic gap is perceived over the last century in this zone, suggesting that the area is stressed and that an earthquake similar to those described above can be expected. Therefore, due to the combination of conditions of exposure and vulnerability which currently exist in San José, these scenarios could be critical in terms of seismic risk, leading to significant human and material losses.

The results described above indicate that the proposed scenarios are both realistic and can be expected if the faults identified are reactivated in the coming years. The probability of the simulated ground motions in this research could be around 10% in 50 years, which coincides with the probability adopted in the seismic code of Costa Rica for conventional housing design (CFIA, 2013). These results can be used to check the spectrum of the construction standard in the country's capital, as well as for the subsequent calculation of seismic risk, which would allow emergency plans and mitigation measures to be developed accordingly. In addition, this analytical approach could be applied in similar regions to identify possible faults which may be close to completing their seismic cycle, as well as in zones with high seismic risk near to densely populated cities.

Declaration of Conflicts of interest

The authors declare no potential conflicts of interest with respect to the research, authorship, and/or publication of this article.

Research Data and Code Availability

The data corresponding to the simulated critical scenarios come from references cited in the text and bibliography. Regarding the local effect and amplification factors: the information corresponding to geology, geotechnics, and geophysics comes from public literature, referenced in the article: Denyer and Arias (1991); Climent and Bolaños (1999); Schmidt et al. (2005); Bogantes (1999); Guzmán (1999); Schmidt and Esquivel-Salas (2023). The Vs30 data used is presented in Table 3 of the article and referenced: Schmidt et al. (2005); Schmidt (2014); IIG Consultants (2017); IIG Consultants (2020). The amplification factors used are detailed in Table 4 of the article, with the corresponding reference: Mixco (2021a and 2021b).

The code employed for the InSAR time series analysis in this manuscript is based on the open-source LiCSBAS package, which is integrated with the LiCSAR automated Sentinel-1 InSAR processor. Detailed information about the LiCSBAS package can be found in the following reference:

- Morishita, Y.; Lazecky, M.; Wright, T.J.; Weiss, J.R.; Elliott, J.R.; Hooper, A. LiCSBAS: An Open-Source InSAR Time Series Analysis Package Integrated with the LiCSAR Automated Sentinel-1 InSAR Processor. Remote Sens. 2020, 12, 424.

Researchers and practitioners can access the LiCSBAS package and its documentation at the corresponding GitHub repository: LiCSBAS GitHub.

The free software used to perform the stress inversion can be downloaded from https://damiendelvaux.be/Tensor/WinTensor/win-tensor_download.html while the MATLAB codes applied to model the slip and dilation tendencies are available at https://www.mathworks.com/matlabcentral/fileexchange/67972-fractend

and https://github.com/DaveHealy-github/FracPaQ

References

Alonso-Henar, J., Montero, W., Martınez-Dıaz, J.J., Alvarez-Gomez. J.A., Insua-Arevalo, J.M., and Rojas, W. (2013). The Aguacaliente Fault, source of the Cartago 1910 destructive earthquake (Costa Rica). Terra Nova, vol. 25, no. 5, pp. 368-373, doi: 10.1111/ter.12045.

Alvarado, G. E., Morales, L. D., Montero, W., Climent, A., and Rojas, W. (1988). Aspectos sismológicos y morfotectónicos del extremo occidental de la Cordillera Volcánica Central, Costa Rica. Rev. Geol. Amér. Central, 9, pp. 75-98.

Alvarado, G. E., and Cordero, M. (2021). Los terremotos en Costa Rica y su influencia en los reglamentos y códigos sísmicos. Rev. Coris, 19, 9-29.

Alvarado, G. E., Benito, B., Staller, A., Climent, Á., Camacho, E., Rojas, W., Marroquín, G., Molina, E., Talavera, J. E., Martínez-Cuevas, S., and Lindholm, C. (2017). The new Central American seismic hazard zonation: Mutual consensus based on up to day seismotectonic framework. Tectonophysics, 721, 462–476. https://doi.org/10.1016/j.tecto.2017.10.013

Angelier, J. (1989). From orientation to magnitudes in paleostress determinations using fault slip data. Journal of Structural Geology, 11(12)):37-50

Araya, M.C., and Biggs, J. (2020). Deformation associated with sliver transport in Costa Rica: seismic and geodetic observations of the July 2016 Bijagua earthquake sequence, Geophysical Journal International, Volume 220, Issue 1, Pages 585–597, https://doi.org/10.1093/gji/ggz474

Arroyo, I. G., and Linkimer, L. (2021). Modelo unidimensional de velocidades sísmicas y características tomográficas tridimensionales del Caribe Sur de Costa Rica. Revista Geológica de América Central, 65, 1–15. https://doi.org/10.15517/rgac.v0i65.46696

Arroyo-Solórzano, M., and Linkimer, L. (2021). Spatial variability of the b-value and seismic potential in Costa Rica. Tectonophysics, 814. https://doi.org/10.1016/j.tecto.2021.228951

Barquero, R. et al. (2009). El terremoto de Cinchona del 8 de enero de 2009, Informe interno. Red Sismológica Nacional (RSN: UCR-ICE), San José, Costa Rica.

Benito, B., Lindholm, C., Camacho, E., Á. Climent, A., Marroquín, G., Molina, E., Rojas, W., Talavera, E., Escobar, J.J., Alvarado, G., Torres, Y., and Perez-Escalante, M. (2010). Amenaza sísmica en América Central, Benito Oterino, B., and Y. Torres Fernández (Editors), Entimema, Madrid, Spain, 371 pp. (in Spanish).

Benito, B., Lindholm, C., Camacho, E., Climent, A., Griselda, M., Molina, E., Rojas, W., Escobar, J., Talavera, E., Alvarado, G., and Torres, Y. (2012). A New Evaluation of Seismic Hazard for the Central America Region. The Bulletin of the Seismological Society of America. 102. 504-523. 10.1785/0120110015.

Blewitt, G., William H., and Kreemer (2018). Harnessing the GPS Data Explosion for Interdisciplinary Science. Eos 99. https://eos.org/project-updates/harnessing-the-gps-data-explosion-for-interdisciplinary-science (last access: January 31, 2023).

Bogantes, R. (1999). Propuesta de zonificación geotécnica para el Área Metropolitana. Informe final de Trabajo de Graduación para optar por el grado de Licenciatura en Ingeniería Civil. Escuela de Ingeniería Civil, Universidad de Costa Rica. San José.

Boore, D., Stewart, J., Seyhan, E., and Atkinson, G. (2014). NGA-West 2 equations for predicting PGA, PGV, and 5 %-Damped PSA for shallow crustal earthquakes. Earthquake Spectra 131108093828003. doi:1

Bourke, J. R., Levin, V., Arroyo, I. G., and Linkimer, L. (2023). Evidence for Caribbean plate subduction in southern Costa Rica. Geology, 51, no. 4, 408–412, doi: 10.1130/G50796.1.

Calderón, A., and Silva, V. (2019) Probabilistic seismic vulnerability and loss assessment of the residential building stock in Costa Rica. Bulletin of Earthquake Engineering 17(3): 1257–1284.

Cauzzi, C., Faccioli, E., Vanini, M., and Bianchini, A. (2015). Updated predictive equations for broadband (0.01–10 s) horizontal response spectra and peak ground motions, based on a global dataset of digital acceleration. Bull Earthquake Eng (2015) 13:1587–1612

CFIA (1987). Código sísmico de Costa Rica 1986. Colegio Federado de Ingenieros y Arquitectos de Costa Rica. Editorial Tecnológica de Costa Rica.

CFIA (2003). Código Sísmico de Costa Rica. Colegio Federado de Ingenieros y Arquitectos de Costa Rica. Editorial Tecnológica de Costa Rica.

CFIA (2013). Lineamientos para el diseño sismorresistente de puentes. Colegio Federado de Ingenieros y Arquitectos de Costa Rica. Editorial Tecnológica de Costa Rica.

CFIA (2022). Informe de Obras sin permiso. Colegio Federado de Ingenieros y Arquitectos de Costa Rica. Inf. Interno CFIA. 44 pp.

Climent, A, Taylor, W., Ciudad Real, M., Strauch, W., Villagran, M., Dahle, A., and Bungum, H. (1994). Spectral strong motion attenuation in Central America. NORSAR Technical Report No. 2-17, 46 pp.

Climent, A., and Bolaños, M. (1999). Mapa de espesores de materiales no consolidados en el Área Metropolitana de San José. Inf. Interno ICE. 12 pp.

COMET (2021). COMET-LiCS Sentinel-1 InSAR portal. https://comet.nerc.ac.uk/comet-lics-portal/

Conejo-Soto, J., and Linkimer, L. (2019). ¡Una ciudad que tiembla! Explorando los sismos urbanos en el área metropolitana de San José. Poster, 3er Congreso Geológico UCR

Crosetto, M., Monserrat, O., Cuevas-González, M., Devanthéry, N., and Crippa, B. (2016). Persistent Scatterer Interferometry: A review. _ISPRS Journal of Photogrammetry and Remote Sensing, 115, 78-89. doi: 10.1016/j.isprsjprs.2015.10.011

Delvaux, D., and Sperner, B. (2003). Stress tensor inversion from fault kinematic indicators and focal mechanism data: the TENSOR program. In: New Insights into Structural Interpretation and Modelling (D. Nieuwland Ed.). Geological Society, London, Special Publications 212, 75-100.

DeMets, C., Gordon, RG., and Argus, D. F. (2010). Geologically current plate motions. Geophysical Journal International, 181:1–80. doi: 10.1111/j.1365-246X.2009.04491.x

Denyer, P., and Arias, O. (1991). Estratigrafía de la Región Central de Costa Rica. En: Rev. Geol. Amér. Central. 12, 1-59.

Denyer, P., and Alvarado, G.E. (2007). Mapa Geológico de Costa Rica, 2007. Escala 1:450 000. Librería Francesa S.A.

Esquivel-Salas, L., Schmidt-Díaz, V., Pittore, M., Hidalgo-Leiva, D., Haas, M., and Moya-Fernández, A. (2022). Remote structural characterization of thousands of buildings from San José, Costa Rica. Front. Built Environ. 8:947329. doi: 10.3389/fbuil.2022.947329

Fan, G., Beck, S., and Wallace, T. (1991). The seismic source parameters of the 1991 Costa Rica aftershock sequence: evidence for a transcurrent plate boundary. J. Geophys. Res., 18, 1385–1388.

Fernández, M., and Rojas, W. (2000). Amenaza sísmica y tsunamis. In Denyer, P. and S. Kussmaul (eds.), Geología de Costa Rica, Editorial Tecnológica de Costa Rica, pp. 287-301.

Ferrill, D. A., Winterle, J., Wittmeyer, G., Sims, D., Colton, S., Armstrong, A., and Morris, A. P.: Stressed rock strains groundwater at Yucca Mountain, Nevada, GSA Today, 9, 1–8, 1999.

Fisher, D., Gardner, T. Sak, P., Sánchez, J., Murphy, K., and Vannucchi, P. (2004). Active thrusting in the inner forearc of an erosive convergent margin, Pacific coast, Costa Rica. En: Tectonics, 23, TC2007, doi:10.1029/2002TC001464.

GEM. (2020). OPENQUAKE ENGINE User Instruction Manual. https://doi.org/10.13117/GEM.OPENQUAKE.MAN.ENGINE.3.9.0

González, P., Walters, R., Hatton, E., Spaans, K., McDougall, A., Hooper, A., and Wright, T. (2016). LiCSAR: Tools for automated generation of Sentinel-1 frame interferograms. AGU Fall Meeting, 2016

Guzmán, J. (1999). Comportamiento dinámico en suelos del Área Metropolitana de San José utilizando técnicas empíricas. Informe final de Trabajo de Graduación para optar por el grado de Licenciatura en Ingeniería Civil. Escuela de Ingeniería Civil, Universidad de Costa Rica. San José.

Healy, D. (2022). FracTend (https://github.com/DaveHealy-github/FracTend), GitHub. Retrieved March 3, 2022.

Healy, D., Rizzo, R., Cornwell, D., Farrell, N., Watkins, H., Timms, N., Gomez-Rivas, E., and Smith, M. (2017). FracPaQ: a MATLAB™ toolbox for the quantification of fracture patterns. Journal of Structural Geology, 95, pp1-16.

Heath, D., Wald, D., Worden, C., Thompson, E., and Scmocyk, G. (2020). A Global Hybrid VS30 Map with a Topographic-Slope-Based Default and Regional Map Insets. Earthquake Spectra, vol. 36, 3: pp. 1570-1584.

Hidalgo-Leiva, D., Linkimer, L., Arroyo, I.G., Arroyo-Solórzano, M., Piedra, R., Climent, A., Schmidt-Díaz, V., Esquivel, L.C., Alvarado, G.E., Castillo, R., et al. (2023). The 2022 Seismic Hazard Model for Costa Rica, Bull. Seismol. Soc. Am. XX, 1–18, doi: 10.1785/0120220119.

IIG Consultores (2017). Prospección geofísica. Sísmica pasiva MAM. Diseño de los intercambios entre la intersección de las rutas nacionales Nº2 Y 236 (Taras), y la intersección de las rutas nacionales Nº 2 y 10 (Cartago) incluyendo el mejoramiento de la ruta nacional Nº2, sección Taras – La Lima (Provincia de Cartago).

IIG Consultores (2020). Estudio geofísico. Sísmica pasiva MAM y sísmica de refracción. estudios de factibilidad técnica, ambiental, social, económica y financiara del fideicomiso corredor vial San José - San Ramón y sus radiales.

INEC (2011). Instituto Nacional de Estadística y Censos. Costa Rica, 2011. Downloaded from www.inec.go.cr/

INEC (2021). Instituto Nacional de Estadística y Censos. Costa Rica. Costa Rica: Población total proyectada al 30 de junio 2021. Downloaded from www.inec.go.cr/

Kanno, T. (2006). A new attenuation relation for strong ground motion in Japan based on recorded data. Bull. Seismol Soc Am 96:879–897. doi:10.1785/0120050138

LaFemina, P., Dixon, T.H., Govers, R., Norabuena, E., Turner, H., Saballos, A., Mattioli, G., Protti, M., and Strauch, W. (2009). Fore-arc motion and Cocos Ridge collision in Central America. Geochem. Geophys. Geosyst. 10(1). doi: 10.1029/2008GC002181.

Lanari, R., Mora, O., Manunta, M., Mallorqui, J. J., Berardino, P., and Sansosti, E. (2004). A small-baseline approach for investigating deformations on full-resolution differential SAR interferograms. _IEEE Transactions on Geoscience and Remote Sensing, 42(7), 1377-1386. doi: 10.1109/TGRS.2004.828196.

Laporte, M., Lindholm, C., Bungum, H., and Dahle, A. (1994). Seismic hazard for Costa Rica. Technical report 2-14, NORSAR. 73 pp.

Lawrence, B. N. , Bennett, V. L., Churchill, J., Juckes, M., Kershaw, P., Pascoe, S., Pepler, S., Pritchard, M., and Stephens, A. (2013) Storing and manipulating environmental big data with JASMIN. In: IEEE Big Data, October 6-9, 2013, San Francisco.

Lazecký, M., Spaans, K., González, P. J., Maghsoudi, Y., Morishita, Y., Albino, F., Elliott, J., Greenall, N., Hatton, E., Hooper, A., Juncu, D., McDougall, A., Walters, R. J., Watson, C. S., Weiss, J. R., and Wright, T. J. (2020). LiCSAR: An Automatic InSAR Tool for Measuring and Monitoring Tectonic and Volcanic Activity. Remote Sensing, 12(15), 2430. doi: 10.3390/rs12152430

Linkimer, L. (2008). Relationship between Peak Ground Acceleration and Modified Mercalli Intensity in Costa Rica. Revista Geológica de América Central, 38: 81-94, 2008. ISSN: 0256-7024

Linkimer, L., Arroyo, G. J., Soto, G., Porras, J. L., Araya, M. C., Mora, M. M., and Taylor, M. (2018). El sismo de Capellades del 2016 y su secuencia sísmica: Manifestación de fallamiento de rumbo en el arco volcánico de Costa Rica, Boletin de Geologia, 40, no. 2, 35–53, doi: 10.18273/revbol.v40n2-2018002.

López, A. (2012). Andersonian and Coulomb stresses in Central Costa Rica and its fault slip tendency potential: new insights into their associated seismic hazard. Geological Society, London, Special Publications, 367, 19-38. doi: 10.1144/SP367.3.

Marshall, J.S., Fisher, D.M. and Gardner, T.W. (2000). Central Costa Rica deformed belt: Kinematics of diffuse faulting across the western Panama block. Tectonics, 19, 468–492.

Matsuoka, M., WAKAMATSU, K., Fujimoto, K., & MIDORIKAWA, S. (2006). Average shear-wave velocity mapping using Japan engineering geomorphologic classification map. *Structural Engineering/Earthquake Engineering*, *23*(1), 57s-68s.

Mescua, J., Durán, P., Porras, H., Giambiagi, L., Moor, M., Cascante, M., Salazar, E., Protti, M. and Poblete, F. (2017). Middle to Late Miocene Contractional Deformation in Costa Rica Triggered by Plate Geodynamics. Tectonics. 36, doi: 10.1002/2017TC004626.

Mixco, L. (2021a). Estimación de Efectos de Sitio a través de Modelos Empíricos. Ministerio de Medio Ambiente y Recursos Naturales (MARN), San Salvador, El Salvador.

Mixco, L. (2021b). Caracterización de tipos de suelo y determinación de factores de amplificación a nivel nacional. Taller de divulgación de insumos técnicos para la actualización de la Normativa Nacional para Diseño y Construcción Sismorresistente en El Salvador. Dirección General de Observatorio de Amenazas y Recursos Naturales, Ministerio del Medio Ambiente, Gobierno de El Salvador, 7 y 9 de septiembre. Downloaded from: http://www.snet.gob.sv/ver/sismologia/riesgo+sismico/riesgo/taller+de+divulgacion+de+insumos+tecnicos/

Monge-Sandí, A. L., 2003. Evaluación de la influencia de los esfuerzos in situ en la excavación de obras subterráneas (aplicado al túnel del P.H Pirrís para la condición de esfuerzos litostáticos). TFG 23364.Tesis de Magister Scientiae en Ingeniería Civil, Universidad de Costa Rica.

Montero, W. (2001). Neotectónica de la región central de Costa Rica: frontera oeste de la microplaca de Panamá. Rev. Geol. Amér. Central, 24: 29–56.

Montero, W., Barahona, M., Rojas, W., and Taylor, M. (2005). Los sistemas de falla Agua Caliente y Rio Azul y relevos compresivos asociados, Valle Central de Costa Rica. Rev. Geol. Amér. Centr, 33: 7-27.

Montero, W. (1999). El terremoto del 4 de marzo de 1924 (Ms 7,0): Un temblor interplaca relacionado al límite oeste de la microplaca de Panamá. Rev. Geol. Am. Centr., 22, pp.21-58

Montero, W., Lewis, J.C., and Araya, M.C. (2017). The Guanacaste Volcanic Arc Sliver of Northwestern Costa Rica. Sci Rep. 2017 May 11;7(1):1797. doi: 10.1038/s41598-017-01593-8. PMID: 28496117; PMCID: PMC5431924.

Montero, W., and Miyamura S. (1981). Distribución de intensidades y estimación de los parámetros focales de los terremotos de Cartago de 1910, Costa Rica, América Central, Revista Instituto Geográfico Nacional. Informe Semestral Julio-Diciembre, pp.9-34.

Montero, W., Soto, G.J., Alvarado, G.E., and Rojas, W. (2010). División del deslizamiento tectónico y transtensión en el macizo del volcán Poás (Costa Rica), basado en estudios neotectónicos y de sismicidad histórica. Rev. Geól. Amér. Central, 43: 13-36.

Montero, W., Rojas, W., and Climent, A. (2016). Modelo de segmentación, estimación de magnitudes y definición de escenarios sísmicos para los sistemas de falla Aguacaliente, Tobosi y Navarro. Informe Final Proyecto CONICIT FI-012-10. 21 págs.

Montero, W., and Rojas, W. (2014). Las fallas Purires y Picagres y su relación con la secuencia sísmica de Puriscal de 1990, Rev. Geol. Amer. Centr., 50: 36-69.

Montero, W., Rojas, W., and Linkimer, L. (2013). Neotectónica de las fallas Ochomogo y Capellades y su relación con el sistema de falla Aguacaliente, falda sur macizo Irazú-Turrialba, Costa Rica. Rev. Geol. Amér. Central, 48: 119-139.

Morell, K., Kirby, E., Fisher, D., and Van Soest, M. (2012). Geomorphic and exhumational response of the Central American Volcanic Arc to Cocos Ridge subduction. Journ. Geophys, Res. 117, doi:10.1029/2011JB008969.

Morishita, Y., Lazecky, M., Wright, T., Weiss, J., Elliott, J., and Hooper, A. (2020). LiCSBAS: An Open-Source InSAR Time Series Analysis Package Integrated with the LiCSAR Automated Sentinel-1 InSAR Processor. Remote Sens., 12, 424.

Morris, A., Ferril, D., and Henderson, B. (1996). Slip-tendency analysis and fault reactivation. Geology, 1996, Vol. 24, Iss: 3, pp 275-278.

Mortgat, C. P., Zsutty, T. C., Shah, H. C., and Lubetkin, L. (1977). A Study of Seismic Risk for Costa Rica (Issue 25).

Murphy J.R., and O'Brien, L.J. (1977). The correlation of peak ground acceleration amplitude with seismic intensity and other physical parameters. Bull. Seismol. Soc. Amer. 67: 877-915.

NEHRP (2020). Recommended provisions for seismic regulations for new buildings and other structures, Part 1: Provisions, FEMA 368, Federal Emergency Management Agency, Washington, D.C.

Peraldo, G., and Montero, W. (1999). Sismología Histórica de América Central. Instituto Panamericano de Historia y Geografía, México, 347 pp.

Portela, J.J., Staller, A., and Bejar, M. (2020). Cortical deformation in the Aguacaliente-Navarro fault system (Central Valley, Costa Rica) from Geodetic data (GNSS and InSAR). EGU2020-12015 https://doi.org/10.5194/egusphere-egu2020-12015.

Protti, M., Güendel, F., and McNally, K. (1995). Correlation between the age of the subducting Cocos Plate and the geometry of the Wadati-Benioff zone under Nicaragua and Costa Rica, in Geologic and Tectonic Development of the Caribbean Plate Boundary in Southern Central America, edited by P. Mann, pp. 309–326. In: Geol. Soc. Am. Spec. Pap. 295, Boulder, Colo.

Rodríguez, E., Linkimer, L., and Montero, W. (2019). Neotectónica de la falla Cipreses, Costa Rica. Boletín de Geología, 41(2): 31-49. Doi: 10.8272/revbol.v41n2-2019002.

Rojas, W., Lindholm, C., Bungum, H., Boschini, I., Climent, A., Barquero, R., Alvarado, G., Soto, G., Montero, W., Fernández, M., Protti, M., Moya, A., Esquivel, L., and Schmidt, V. (1998). Seismic hazard analysis for the Metropolitan Area of the Central Valley, Costa Rica.

Technical Report, Phase II, Reduction of Natural Disasters in Central America Project. Norsar, Norway. October 1998. 59 pp.

Rojas, W., Montero, W., Schmidt, V., and Leandro, G. (2005). Estudio de amenaza sísmica para las doce ciudades más importantes de Costa Rica. Informe particular de FUNDEVI-UCR para el INS, Univ. Costa Rica, 190 pp.

Röckel L. , Ahlers S. , Müller B. , Reiter K. , Heidbach O., Henk A., Hergert T., and Schilling F. (2022). The analysis of slip tendency of major tectonic faults in Germany. EGU-Solid Earth. Volume 13, issue 6, SE, 13, 1087–1105, 2022. doi: 10.5194/se-13-1087-2022.

Red Sismológica Nacional de Costa Rica (RSN). (2021). The Costa Rica National Seismological Network Catalog during 1975-2020. doi: 10.15517/TC

Sak, P. B., Fisher, D., Gardner, T., Marshall, J., and LaFemina P. (2009). Rough crust subduction, forearc kinematics, and Quaternary uplift rates, Costa Rican segment of the Middle America Trench. In: Geol. Soc. Am. Bull., 121(7/8), 992–1012, doi:10.1130/B26237.1.

Salgado-Gálvez, M. A., Ordaz, M., Singh, S. K., Pérez-Campos, X., Huerta, B., Bazzurro, P., and Fagà, E. (2022). A Caribbean and Central America Seismic Hazard Model for Sovereign Parametric Insurance Coverage, Bull. Seismol. Soc. Am. 113, 1–22, doi: 10.1785/0120220117

Scherbaum, F., Cotton, F., and Smit, P. (2004). On the use of response spectra reference data for the selection of ground motion models for seismichazard analysis in regions of moderate seismicity: The case of rock motion. Bull. Seismol. Soc. Am. 94, no. 6, 2164–2185

Schmidt, V., Dahle, A., and Bungum, H. (1997). Costa Rican spectral strong motion attenuation, NORSAR, Technical Report, 45 pp

Schmidt, V. (2014). Clasificación de suelos de 15 estaciones acelerográficas, mediante el uso de métodos basados en vibraciones ambientales y del parámetro Vs30. Revista Geológica de América Central, 51(1). doi: 10.15517/rgac.v51i1.16850

Schmidt, V., Moya, A., Climent, A., Rojas, W., and Boschini, I. (2005). Microzonificación sísmica de San José, Costa Rica. Ed. de la Univ. de Costa Rica.

Schmidt-Díaz, V. and Esquivel-Salas, L.C. (2023). Periodo fundamental y clasificación de sitios en el cantón Central de San José (Costa Rica) usando la técnica H/V. Revista Geológica de América Central, 68, 1-17. doi: 10.15517/rgac.2023.55170

Stirling, M., Rhoades, D., and Berryman, K. (2002), Comparison of Earthquake Scaling Relations Derived from Data of the Instrumental and Preinstrumental Era, Bull. Seism. Soc. Am. 92, no.

Trifunac, M.D. and Brady, A.G., (1975). On the correlation of seismic intensity scale with the peaks of recorded strong ground motion , Bull. Seismol. Soc. Amer. 65: 139-162.2, 812–830.

Stirling, M., Goded, T., Berryman, K., and Litchfield, N. (2013), Selection of earthquake scaling relationships for seismic-hazard analysis, Bull. Seism. Soc. Am. 103, no. 6, 2993–3011, doi: 10.1785/0120130052.Wells, D. L., & Coppersmith, K. J. (1994). New empirical relationships among magnitude, rupture length, rupture width, rupture area, and surface displacement. Bulletin of the seismological Society of America, 84(4), 974-1002.

Tables

Table 1. Kinematic and geometric characteristics of the three critical fault scenarios near San José.

Fault	Long.	Lat.	Strike (°)	Dip (°)	Rake (°)	Fault Type	Mw	Length (km)	Width (km)	Rrup* (km)
Belo Horizonte	-84.138	9.861	135	30	45	Sinistral-Reverse	6.2	12.6	7.0	5
Río Azul	-84.018	9.889	85	90	45	Sinistral	6.6	15.4	15.0	5.2
Cipreses	-83.963	9.964	330	25	45	Reverse-Sinistral	6.3	14.0	9.2	4.3

* closest distance to the rupture surface

Table 2. Applicability ranges of the GMPEs used in the ground motion estimation.

GMPE Model	Abbreviation	Dataset	Magnitude range (Mw)	Response spectra range (s)	Distance Rrup range (km)
Cauzzi et al. (2015)	CA14	Global acceleration records	4.5 – 7.9	0 – 10	< 150
Kanno et al. (2006)	KA06	Records from Japan, USA, and Turkey	6.0 – 8.0	0 – 5	< 200
Boore et al. (2014)	BO14	California, Taiwan, Japan, China, Italy, Greece, Turkey, and Alaska.	3.0 – 7.9	0.01 - 10	< 400

Table 3. Points with Vs30 data compiled for this study.

Latitude	Longitude	Vs30 (m/s)	NEHRP classification	Zone	Reference
-84.061	9.943	251	D	Z1	Schmidt et al., (2005)
-84.070	9.935	276	D		
-84.087	9.932	276	D		
-84.123	9.945	224	D		
-84.169	9.994	233	D		
-84.106	9.922	286	D		
-84.035	9.926	164	DE		
-84.103	9.936	153	DE		
-84.049	9.888	226	D		
-84.064	9.899	312	CD		
-84.107	9.945	564	C	Z1	IIG Consultores (2020)
-84.111	9.949	283	D		
-84.115	9.955	417	CD		
-84.128	9.964	322	CD		
-84.134	9.967	510	C		
-84.140	9.970	350	CD		
-84.190	10.000	297	D	Z2	
-84.206	10.000	443	C		
-84.235	9.995	341	CD		
-84.268	9.996	436	CD		
-84.295	10.006	315	CD		
-84.097	9.915	380	CD	Z1	Schmidt (2014)
-84.203	9.950	696	C		
-84.099	9.935	302	D		
-84.053	9.935	347	CD		
-84.044	9.937	340	CD		
-84.044	9.945	283	D		
-84.193	10.137	152	DE	Z2	
-83.927	9.864	267	D		
-83.869	9.827	269	D		
-83.907	9.854	377	CD		
-84.036	9.995	279	D		
-84.036	9.995	279	D		
-84.117	10.000	432	CD		
-84.243	9.924	263	D		
-84.036	9.869	263	D		
-84.266	10.008	284	D		
-83.924	9.863	244	D		
-84.193	10.137	152	DE		
-83.936	9.884	258	D	Z2	IIG Consultores (2017)
-83.943	9.876	267	D		
-83.944	9.868	282	D		

Table 4. Amplification factors for each soil class and different PGA values (Mixco, 2021).

Soil type	**PGA (g)**																					
	0.01	**0.05**	**0.10**	**0.15**	**0.20**	**0.25**	**0.30**	**0.35**	**0.40**	**0.45**	**0.50**	**0.55**	**0.60**	**0.65**	**0.70**	**0.80**	**0.90**	**1.00**	**1.50**	**2.00**	**2.50**	**3.00**
BC	1.14	1.24	1.27	1.27	1.27	1.27	1.27	1.26	1.26	1.25	1.25	1.25	1.24	1.24	1.23	1.23	1.22	1.22	1.21	1.21	1.09	1.09
C	1.30	1.33	1.32	1.30	1.28	1.27	1.25	1.24	1.23	1.22	1.21	1.20	1.19	1.18	1.17	1.16	1.15	1.13	1.12	1.12	1.04	1.04
CD	1.51	1.53	1.48	1.45	1.42	1.39	1.37	1.35	1.33	1.31	1.30	1.29	1.27	1.26	1.25	1.23	1.22	1.20	1.19	1.19	0.98	0.98
D	1.93	1.71	1.59	1.52	1.47	1.43	1.40	1.37	1.35	1.33	1.31	1.30	1.28	1.27	1.26	1.23	1.22	1.20	1.16	1.14	0.98	0.98
DE	2.72	1.99	1.70	1.55	1.45	1.37	1.32	1.27	1.23	1.20	1.17	1.15	1.12	1.10	1.09	1.06	1.03	1.00	0.98	0.98	0.98	0.98
E	2.13	1.55	1.25	1.08	0.96	0.86	0.79	0.72	0.66	0.61	0.57	0.53	0.49	0.46	0.42	0.37	0.32	0.28	0.24	0.24	0.24	0.24

Soil type	**Sa (g); T= 0.1 s**																					
	0.01	**0.05**	**0.10**	**0.15**	**0.20**	**0.25**	**0.30**	**0.35**	**0.40**	**0.45**	**0.50**	**0.55**	**0.60**	**0.65**	**0.70**	**0.80**	**0.90**	**1.00**	**1.50**	**2.00**	**2.50**	**3.00**
BC	1.17	1.18	1.19	1.20	1.20	1.19	1.19	1.19	1.18	1.18	1.17	1.17	1.17	1.16	1.16	1.15	1.15	1.14	1.12	1.10	1.19	1.18
C	1.25	1.29	1.33	1.35	1.35	1.34	1.34	1.33	1.33	1.32	1.31	1.31	1.30	1.30	1.29	1.28	1.27	1.26	1.21	1.19	1.06	1.05
CD	1.34	1.37	1.41	1.42	1.41	1.40	1.38	1.37	1.35	1.34	1.32	1.31	1.30	1.29	1.28	1.26	1.24	1.22	1.17	1.15	0.98	0.98
D	1.53	1.52	1.55	1.52	1.49	1.46	1.42	1.40	1.37	1.34	1.32	1.30	1.28	1.26	1.25	1.22	1.19	1.16	1.11	1.08	0.79	0.77
DE	1.75	1.75	1.74	1.67	1.60	1.54	1.48	1.42	1.37	1.33	1.28	1.25	1.21	1.18	1.15	1.09	1.04	1.00	0.93	0.91	0.91	0.91
E	1.48	1.43	1.23	1.11	1.02	0.95	0.89	0.84	0.80	0.76	0.73	0.69	0.66	0.64	0.61	0.56	0.52	0.48	0.34	0.23	0.14	0.11

Soil type	**Sa (g); T= 0.2 s**																					
	0.01	**0.05**	**0.10**	**0.15**	**0.20**	**0.25**	**0.30**	**0.35**	**0.40**	**0.45**	**0.50**	**0.55**	**0.60**	**0.65**	**0.70**	**0.80**	**0.90**	**1.00**	**1.50**	**2.00**	**2.50**	**3.00**
BC	1.09	1.14	1.16	1.17	1.17	1.17	1.17	1.18	1.18	1.17	1.17	1.17	1.17	1.17	1.17	1.17	1.17	1.17	1.16	1.16	1.11	1.11
C	1.34	1.35	1.32	1.30	1.29	1.28	1.27	1.26	1.26	1.25	1.24	1.24	1.23	1.23	1.23	1.22	1.21	1.21	1.17	1.16	1.13	1.13
CD	1.52	1.53	1.55	1.54	1.52	1.51	1.49	1.48	1.46	1.45	1.43	1.42	1.41	1.40	1.39	1.37	1.35	1.33	1.25	1.23	1.16	1.16
D	1.66	1.80	1.80	1.75	1.69	1.64	1.58	1.54	1.49	1.45	1.41	1.38	1.34	1.31	1.28	1.23	1.19	1.16	1.09	1.09	1.07	1.07
DE	2.45	2.42	2.27	2.12	2.00	1.90	1.81	1.73	1.67	1.61	1.55	1.50	1.46	1.42	1.38	1.31	1.25	1.19	1.02	1.02	1.02	1.02
E	2.26	2.19	1.84	1.64	1.49	1.39	1.30	1.22	1.16	1.10	1.05	1.00	0.96	0.92	0.88	0.82	0.76	0.71	0.51	0.38	0.27	0.27

Soil type	**Sa (g); T= 1.0 s**																					
	0.01	**0.05**	**0.10**	**0.15**	**0.20**	**0.25**	**0.30**	**0.35**	**0.40**	**0.45**	**0.50**	**0.55**	**0.60**	**0.65**	**0.70**	**0.80**	**0.90**	**1.00**	**1.50**	**2.00**	**2.50**	**3.00**
BC	1.11	1.13	1.13	1.13	1.13	1.13	1.13	1.13	1.13	1.13	1.13	1.13	1.13	1.13	1.13	1.14	1.14	1.14	1.13	1.13	1.02	1.02
C	1.23	1.19	1.16	1.14	1.13	1.12	1.11	1.11	1.10	1.10	1.09	1.09	1.08	1.08	1.08	1.07	1.07	1.06	1.04	1.03	1.12	1.12
CD	1.58	1.56	1.56	1.55	1.55	1.55	1.55	1.55	1.55	1.55	1.55	1.54	1.54	1.54	1.54	1.54	1.54	1.54	1.54	1.54	1.45	1.45
D	2.15	2.17	2.14	2.11	2.09	2.06	2.04	2.03	2.01	2.00	1.98	1.97	1.96	1.94	1.93	1.91	1.89	1.88	1.81	1.75	1.88	1.88
DE	2.19	2.38	2.44	2.47	2.49	2.50	2.51	2.51	2.51	2.51	2.51	2.51	2.51	2.51	2.51	2.51	2.51	2.51	2.51	2.51	2.51	2.51
E	3.45	2.85	2.44	2.16	1.95	1.77	1.63	1.63	1.63	1.63	1.63	1.63	1.63	1.63	1.63	1.63	1.63	1.63	1.63	1.63	1.63	1.63

Table 5. Metrics for the deformation information over the area of the faults (mm/yr).

Fault	**Min**	**Max**	**P05**	**P95**	**Mean**
Belo Horizonte	-3.4	2.4	-1.2	1.7	0.3
Cipreses	-3.5	2.5	-1.1	1.3	0.2
Río Azul	-3.1	2.8	-2.0	1.3	-0.1